Properties and Functions of I_h in Hippocampal Area CA3 Interneurons

by

Warren D. Anderson

B.A., Temple University, 2006

Submitted to the Graduate Faculty of

Arts and Sciences in partial fulfillment

of the requirements for the degree of

Master of Science

University of Pittsburgh

2009

UNIVERSITY OF PITTSBURGH

School of Arts and Sciences

This thesis was presented

by

Warren D. Anderson

It was defended on

July, 15 2009

and approved by

Jon Johnson, Ph.D., Department of Neuroscience

Stephen Meriney, Ph.D., Department of Neuroscience

German Barrionuevo, M.D., Department of Neuroscience (Chair)

Properties and Functions of I_h in Hippocampal Area CA3 Interneurons

Anderson, BA

University of Pittsburgh, 2009

Abstract

I_h is an important contributor to the subthreshold membrane properties of various mammalian neurons, including interneurons. Here I characterize the properties of I_h in a subpopulation of hippocampal area CA3 interneurons with somata in *stratum radiatum* and *stratum lacunosom moleculare*. As shown in previous studies, I_h in these cells has sigmoidal voltage dependence of activation with kinetics characterized by two exponential components for both channel activation and deactivation. Interestingly, the activation and deactivation kinetics were most aptly described by distinct functions of voltage. These results were incorporated into a novel biophysical model of I_h that was applied in single compartment model simulations and dynamic clamp experiments. Finally, I assessed the functional consequences of I_h by examining the effects of this current on subthreshold temporal summation of mossy fiber EPSPs as well as frequency dependent neuronal responses. My results show that I_h decreases temporal summation of mossy fiber EPSPs but does not impart resonance in CA3 interneurons at potentials where I_h is active.

TABLE OF CONTENTS

LIST OF TABLES

LIST OF FIGURES

PREFACE

Acknowledgements:

Thanks first to my family for all the support: Mom, Dad, Granddad, Grammy, Chris, Suhailah, and Jamal, and all my aunts, uncles, and cousins. Thank you to my committee for all of the valuable input: Jon, Steve, and German. Extra special thanks to Jon for invaluable advice on the construction and description of the mathematical model for I_h as well as extensive commenting on the text of this document. Thanks to everyone in the neuroscience department for making everything go smoothly: Joan, Marlene, Jim, Frank, and Joe, and everybody in the fiscal department. Thanks to Linda and John for advising my rotations along with everybody in their labs: Layla, Mike, Vicky, Katrina, Ilva, Stacey, and extra thanks to Paul Kullmann for teaching me so much (as well as setting up the dynamic clamp software). Thanks to Pat and Floh for helping out with the immunolabelling. Thank you so much to German and everyone in the lab I got to work with for 3 years: Kate, Emilio, Tamara, Nate, and John. Extra thanks to my good friends Freddy and Josh for coming out to visit and all the olde time hommies: Paul, Ryan, Dun, the Horans, Jono, Greg, the Steeles, Emmanual, Jason, Reece, the Swishers. Lastly, cheers to all my friends in PGH: Cosgrove, Jesse, Nicky, Shawn, Darwin, Erica, Drew, Mike, Dan, Layla, Erika J, Tom, Thom, DJ, Jen.

Abbreviations:

EC: The entorhinal cortex
DG: The dentate gyrus
CA3: Area CA3 of the mammalian hippocampus
CA1: Area CA1 of the mammalian hippocampus
MF: The mossy fiber pathway
PP: The perforant pathway
RC: The recurrent collateral pathway
SLM: Stratum lacunosom moleculare
SR: Stratum radiatum
SL: Stratum lucidum
SP: Stratum pyrimadale
SO: Stratum oriens
SAN: Sinoatrial node
LTP: Long-term synaptic potentiation

EPSC: Excitatory postsynaptic current
EPSP: Excitatory postsynaptic potential
cAMP: cyclic adenosine monophosphate
HCN: Hyperpolarization-activated cyclic nucleotide gated
HH model: The classic Hodgkin-Huxley model formulation
V_{rest}: The resting membrane potential
τ_m: The passive membrane time constant
Z: Frequency dependent impedance
|Z|: Impedance magnitude
FFT: Fast Fourier transform
f_r: Resonant frequency

1.0 INTRODUCTION

1.1 THE HIPPOCAMPUS AND MEMORY

Behavioral experiments and clinical cases provide convergent evidence for a critical role of the mammalian hippocampus in memory (Eichenbaum & Otto, 1992). Theoretical accounts of hippocampal function based on both anatomical and physiological data suggest that hippocampal area CA3 is the initial locus of associative memory storage and recall (see Fig 1 for an illustration of hippocampal anatomy). Cortical inputs that represent "events" to be remembered are propagated to CA3 via the perforant pathway (PP) and the mossy fibers (MFs). Axons from entorhinal cortex principal cells constitute the PP which has terminations on both dentate gyrus (DG) and CA3 neurons. MFs are axons that project from DG granule cells to both pyramidal cells and inhibitory interneurons in CA3 (e.g., Acsády et al., 1998). Thus, cortical representations are relayed to CA3 pyramidal neurons monosynaptically via the PP input and disynaptically via the MF pathway. The active "cell assembly" or constituent of CA3 pyramidal cells activated by a given cortical input (Hebb, 1949) constitutes CA3's representation of cortical information to be remembered.

Anatomical analyses of CA3 have demonstrated that this region is organized such that its principal neurons are interconnected by recurrent axon collaterals (RCs, e.g., Amaral & Witter, 1995). This anatomical arrangement has been proposed to provide a substrate for “autoassociative” memory (Hopfield, 1982; Marr, 1971; McNaughton & Morris, 1987; Rolls, 1989). Autoassociative memories are instantiated by the process of autoassociation: the enhancement of connection strengths between interconnected neurons that are mutually activated by a given input (e.g., McNaughton & Morris, 1987; McNaughton & Nadel, 1990). Another feature of autoassociative memory is that a “partial cue” of the original cortical input pattern, i.e., spiking in a subset of the input fibers that originally evoked the memory, is sufficient to reinstitute the stored memory. Reactivation of a stored memory consists of activity in the original cell assembly that represented the remembered event at the initial time of storage. Long term potentiation (LTP) of RC synapses between coactive units of a given cell assembly is believed to provide the biological basis for both the storage and recall of autoassociative memories (Marr, 1971; McNaughton & Morris, 1987; Treves & Rolls, 1994). According to this theory the induction of LTP at RC synapses constitutes memory storage and the assembly reactivation process results in recall. When a partial cue of the original cortical input is activated, a small subset of the originally activated assembly is activated and the firing of these cells leads to EPSPs at potentiated RC synapses on other cells that represented the event. Stimulation of these potentiated synapses will result in firing of more cells representing the event and the whole assembly will eventually be reactivated by iterative activation of potentiated RC synapses. This recall process is referred to as “pattern completion” (O’Reilly & McClelland, 1994; Treves & Rolls, 1994). Thus, the RC synapses might function as a matrix for autoassociative memory storage and recall (McNaughton & Morris, 1987; McNaughton & Nadel, 1990).

The memory capacity of a neural network such as CA3 depends on several factors including the number of units in the network, the sizes of the memory representations, and the number or RC synapses on a given pyramidal cell (Treves & Rolls, 1992, 1994). Due to these capacity constraints, mechanisms that support the “sparsification” and “pattern separation” of memory representations have been proposed to enhance the mnemonic capacity of CA3 (Marr, 1971; McNaughton & Nadel, 1990; O’Reilly & McClelland, 1994; Rolls & Treves, 1998; Treves & Rolls, 1992, 1994). The sparsification of cortical input entails the compression of a cortical representation such that the proportion of pyramidal neurons active in CA3 is reduced as much as possible for each memory. Pattern separation refers to the decorrelation or orthogonalization of the patterns so that events represented by overlapping populations of cortical inputs are represented in CA3 by cell assemblies with less overlap. The sparsification and pattern separation of cortical inputs are believed to be accomplished by the DG.

Three characteristics of DG and the MF pathway are consistent with the sparsification and/or pattern separation functions of this hippocampal subdivision. First, the input to CA3 from the MF pathway is relatively sparse compared to the relatively diffuse PP projection: each CA3 pyramidal neuron receives ~50 MF synapses and ~4000 PP inputs and each granule cell’s projection is estimated to contact only 14 pyramidal cells (Amaral et al., 1990). Hence, the low convergence and divergence of the MF pathway entails sparse connectivity from DG to CA3 which is believed to contribute to representation sparsification. Second, the DG contains approximately 4-6 times the number of principal neurons in EC or CA3 (see Amaral & Witter, 1995; Boss et al., 1995, 1987) and the proportion of granule cells active is lower on average than in EC or CA3 (Jung & McNaughton, 1993, see also O’Reilly & McClelland, 1994). The propagation of information from EC to DG therefore results in relaying a signal from one space to a relatively larger space (i.e., a higher dimensional space) where firing is sparse, which has been shown in theoretical analyses to enhance pattern separation (Marr, 1969). The final reason that DG is proposed to enforce sparcification and pattern separation is that the set of active granule cells is believed to determine the set of active CA3 pyramidal cells.

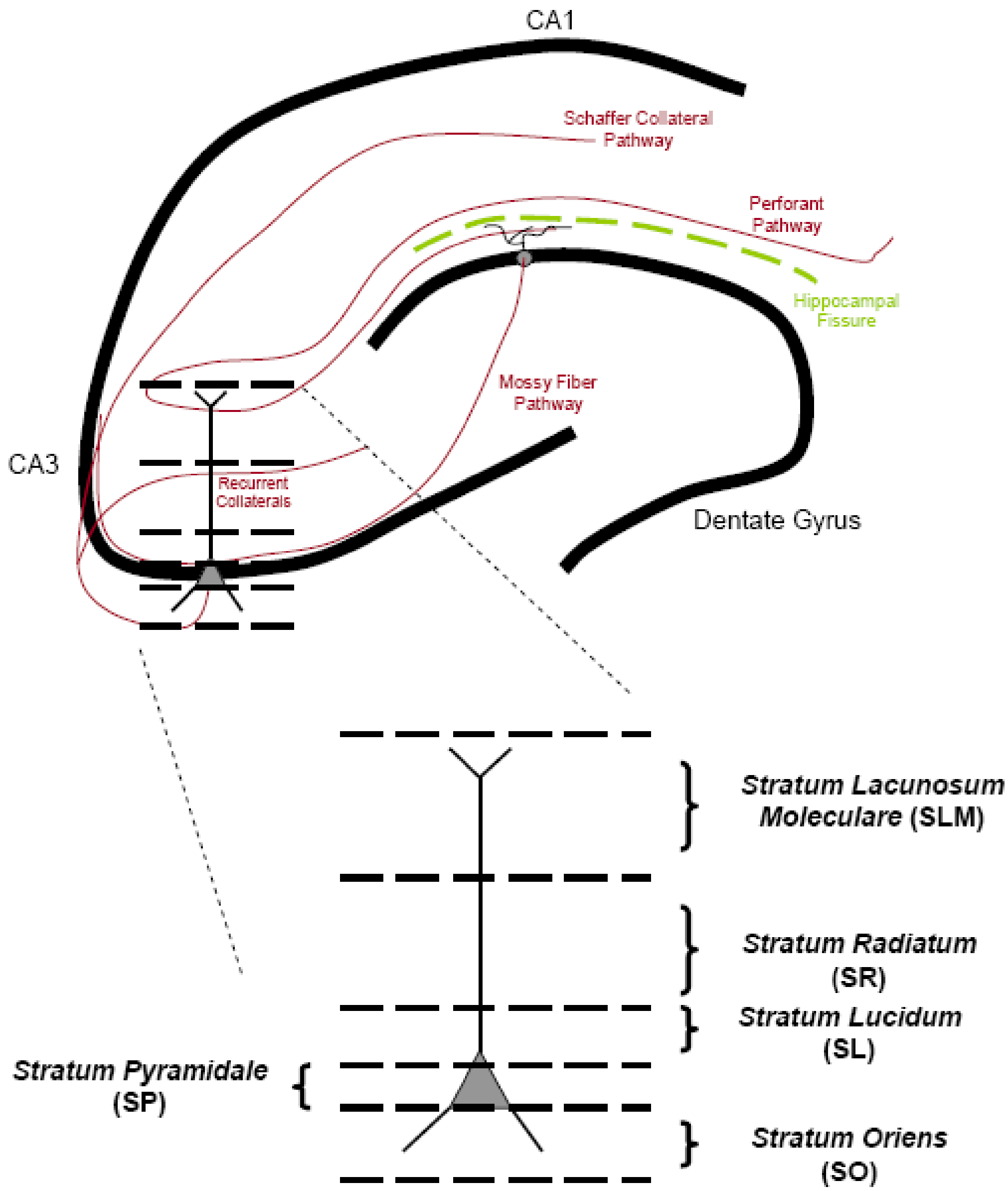

Figure 1. *The fiber pathways and laminar structure of the rat hippocampus.* The schematic at the top shows an illustration of a transverse section of rat hippocampus. The major subdivisions include the dentate gyrus (DG), CA3, and CA1. The major inputs to CA3 include the mossy fiber pathway (MF) and the perforant pathway (PP). The designations for the various layers of the hippocampus are shown below.

MF inputs to CA3 pyramidal cells are sparse and strong relative to PP inputs. Each pyramidal neuron in CA3 receives PP inputs at the distal portion of the apical dendrite while these cells receive MF synapses on proximal apical dendrites (within ~100 µm from somata, e.g., Henze et al., 2000). Hence, because of the relatively short electrotonic distance between MF synapses and the perisomatic spike triggering zone in the axon (Meeks & Mennerick, 2007), it was proposed that these synapses are very efficacious (Blackstad & Kjaeheim, 1961). Both *in vitro* and *in vivo* electrophysiological data also indicate that MF inputs are particularly strong. Mori and Colleagues (2004) obtained paired whole cell recordings from DG granule cells and CA3 pyramidal neurons in organotypic slice cultures and found that the AMPA receptor mediated EPSC was -163 ± 23 pA at -70 mV, whereas minimal stimulation of RC and PP inputs has been found to evoke -11.8 ± 4.8 and -6.61 ± 2 pA responses on average, respectively, in CA3 pyramidal neurons at -80 mV (Perez et al., in preparation). Extracellular recordings from CA3 pyramidal cells during granule cell action potential trains evoked by intracellular stimulation *in vivo* further indicate that stimulation of a single granule cell is sufficient to evoke spiking in CA3 neurons for frequencies within the gamma band (20-100 Hz, Henze et al., 2002). These findings provide evidence for the hypothesis that the MF input functions as a “detonator” of cells within CA3. According to theory, MF inputs select the cell assembly during information transfer from cortex to hippocampus by virtue of the exceptionally strong MF synapses (McNaughton & Morris, 1987; Treves & Rolls, 1994). This detonator function allows the active set of granule cells to determine the cells to be active in CA3 and effectively enforce pattern separation because of the sparcity of the MF projection (see Treves & Rolls, 1992).

To summarize the theoretical and computational accounts of the hippocampal memory encoding and recall mechanisms, the principal role of the DG is to control sparse encoding and pattern separation in order to promote maximal memory capacity and the RC system in CA3 allows for successful recall of memories stored by enhancements of RC synapses. DG promotes sparsity in CA3 because the neural code in DG is sparse, the MF pathway has both low divergence and low convergence in CA3, and the firing of DG cells determines the active assembly in CA3. Pattern separation occurs in DG as a result of the low activity levels in this region and is enhanced in CA3 by the sparse connectivity of the MF pathway. Sparse connectivity promotes pattern separation because each CA3 pyramidal cell receives input from very few DG cells and small changes in a granule cell assembly constituents will result less assembly overlap in CA3 (Rolls, 1989). The activation of a subset of an assembly that previously represented a memory will reactivate the entire assembly by sequentially activating more and more of the enhanced RC synapses. However, an interesting feature of these analyses is that the primary role assigned to inhibitory interenurons was control of activity levels.

1.2 HIPPOCAMPAL AREA CA3 INTERNEURONS

The rat hippocampus contains a variety of interneurons that can be differentiated based on various factors including morphology, neurochemistry, electrophysiological properties, and/or neuromodulator receptor expression (e.g., Freund & Buzsaki, 1996; Klausberger & Somogyi, 2008; Parra et al., 1998). While a substantial degree of progress has been made in classifying CA1 interneurons and characterizing the functional roles of various interneurons in controlling network behavior (e.g., see Klausberger & Somogyi, 2008 for a review), comparatively less data on the properties and functions of CA3 interneurons are available. My experiments contribute to bridging this gap by characterizing some of the electrophysiological properties of CA3 interneurons that have been previously been delineated by their axon projection geometry (Ascoli et al., 2009).

The fact that different classes of hippocampal neurons contact distinct dendritic domains of CA3 pyramidal cells might suggest that there is an association between the dendritic termination zone and the computational function of a given interneuron. For instance, somatic inhibition might promote the precisely timed repression of firing while dendritic inhibition decreases the efficacy of dendritic inputs by suppressing dendritic calcium spikes (see Miles at al., 1996). While many interneurons with somata in the *stratum pyramidale* (SP) and *stratum lucidum* (SL) layer of CA3 (see Fig 1) contact perisomatic regions of CA3 pyramidal cells (Vida & Frotscher, 2000; see also Hajos et al., 2004 Figs 4 and 5), interneurons in *stratum radiatum* (SR) and *stratum lacunosom moleculare* (SLM) project towards dendritic domains of CA3 pyramidal cells (Ascoli et al., 2009). Because RC synapses are located within SR, the SR and SLM interneurons may influence memory storage and/or recall by regulating dendritic electrogenesis in the domain of the RC input.

SR/SLM interneurons in CA3 receive excitatory input from the PP, MF, and RC pathways (Calixto et al., 2008; Perez-Rosello & Barrionuevo, 2007), and hence these neurons are anatomically suited to provide both feedforward and feedback inhibition to CA3 pyramidal cell dendrites. Thus, these inhibitory inputs might impose control over both pattern separation and pattern completion. For instance, precisely timed feedforward inhibition during memory storage might enhance sparsity and pattern separation by preventing the LTP induction at RC synapses following MF/PP inputs to SR/SLM interneurons and pyramidal cells. During recall (pattern completion), feedback inhibition might help to reduce the feedback excitation of the collateral system which could both prevent the induction of epileptiform activity and reduce the activation of cells that were not part of the original assembly that represented the memory to be recalled. The roles of these interneurons in controlling network activity in CA3 and its mnemonic functions will depend on the spiking properties of these cells. In particular, the subthreshold voltage and time dependent membrane properties of SR/SLM interneurons will determine the characteristics of synaptic integration in these cells. In turn, the characteristics of synaptic integration will influence the spiking properties of these interneurons (Konig et al., 1996). These integrative characteristics are determined by a plethora of factors including synapse location, synaptic conductance and kinetics, neuronal geometry, both passive and active membrane properties, and interactions between the aforementioned factors (e.g., Llinas, 1988; Magee, 2000; Mainen & Sejnowski, 1996; Rall, 1977; Spruston et al., 1999). The focus of my study was to examine the influence of active properties on subthreshold properties of CA3 SR/SLM interneurons.

1.3 THE H-CURRENT

The present study was designed to investigate the influence of the hyperpolarization activated inward current I_h on subthreshold membrane properties. The significance of I_h is exemplified by the fact that this current has been shown to have important effects on both synaptic integration (e.g., Magee, 1999) and oscillatory behavior (e.g., Dickson 2000) in neurons, as described further below. Noma and Irisawa (1976) first showed that hyperpolarization of heart sinoatrial node (SAN) cells from -35 mV in voltage clamp resulted in a slowly developing inward current. In current clamp the application of hyperpolarizing steps resulted in a depolarizing “sag” in the membrane potential following the initial voltage deflection. A more detailed voltage clamp characterization of this hypolarization activated current in cardiac purkinje fibers was later provided by DiFrancesco (1981) who found that this current had a reversal potential positive to -50 mV that was sensitive to changes in Na^+ and K^+ concentrations. The current also activated as a sigmoidal function of voltage that increased with hyperpolarization. These results suggested that this current, termed I_f in cardiac cells ("f" was for "funny current" because it was comical to the authors that the current activated with hyperpolarization), was mediated by channels permeable to Na^+ and K^+ and opened with increased probability at potentials negative to -50 mV. A hyperpolarization-activated current similar to I_f was later found in current and voltage clamp studies of retinal neurons (Bader et al., 1982) and the authors referred to this current as I_h. The designation I_h was subsequently adopted as the title for currents in neurons with biophysical properties similar to those of I_f. Evidence for a hyperpolarization activated inward current was also found in hippocampal pyramidal neurons based on voltage clamp analyses (Halliwell & Adams, 1982). Subsequently, Maccaferri and colleagues (1993) assessed the voltage dependence and reversal potential of I_h in hippocampal CA1 neurons by blocking the h-conductance with Cs^+ and using the Cs^+-sensitive voltage clamp current traces for all I_h measurements. The most extensive characterization of the biophysical properties of I_h in CA1 neurons was later completed by Magee (1998).

A signature feature of I_f and I_h is that the voltage dependence of the conductance and kinetics are modulated by cyclic nucleotides. It was originally found that I_f increases following adrenaline or norephinephrine (NA) administration to SAN cells, though the mechanism(s) of this modulatory effect were initially illusive (Brown et al., 1979; DiFrancesco et al., 1986). In contrast, DiFrancesco and Tromba (1988a) found that ACh decreases SAN I_f and the mechanism was determined to be a decrease in cAMP following G-protein coupled (muscarinic) ACh receptor stimulation mediated inhibition of adenylate cyclase (DiFrancesco & Tromba, 1988b). Difrancesco and Tortora (1991) later showed that cAMP shifts the voltage dependence of I_f activation in the depolarizing (i.e., rightward) direction and accelerates current kinetics by mechanisms that do not require protein kinase mediated phosphorylation, which suggested that cAMP might bind directly to the channels. These results indicate that NA increases I_f by a β-adreneric receptor-dependent increase in adenylate cyclase activity resulting in cAMP production (Difrancesco & Tortora, 1991; DiFrancesco & Tromba, 1988b). The effect of acetylcholine, in contrast, appears to be a muscarinic receptor-dependent decrease in cAMP synthesis mediated by adenylate cyclase inhibition (DiFrancesco & Tromba, 1988b).

Modulation has also been shown to be prominent in neuronal I_h. Consistent with the results for I_f, NA and cAMP were both found to increase the voltage dependence of I_h activation in auditory neurons from by shifting the activation curve in the depolarizing direction (Banks et al., 1993). In addition, 5-HT was also found to increase I_h, likely due to an increase in cAMP (Bobker & Williams, 1989). These findings were also replicated in other cells, thalamic neurons for example (McCormick & Pape, 1990), and a variety of other signaling molecules have been shown to modulate the biophysical properties of I_h (e.g., Pape, 1996).

The correspondence between the biophysical and modulatory properties of I_f and I_h suggested that these currents might have similar molecular substrates. Evidence for this hypothesis was provided in 1998 when three groups independently cloned genes that produced currents that resemble I_f/I_h in terms of the biophysical properties and cAMP sensitivity when expressed in heterologous systems (Ludwig et al., 1998; Gauss et al., 1998; Santoro et al., 1998). These efforts resulted in the cloning of cDNA encoding four protein subunits, HCN1-4 (HCN denotes *h*yperpolarization-activated, *c*yclic *n*ucleotide gated channel proteins, Clapham, 1998), which were then used for studying the biophysical properties of I_f/I_h in expression systems and labeling of the HCN channels in the brain and heart. Northern blot, *in situ* hybridization, and/or immunohistochemical labeling for HCN subunits indicated that expression patterns accord well with electrophysiological findings, thus suggesting that native I_f and I_h are both composed of HCN proteins (Santoro & Tibbs, 1999; Robinson & Seigelbaum, 2003). Several biophysical analyses have been applied to homomers composed of HCN subunits. These analyses suggest that the kinetics of activation are faster for HCN1 than HCN2 and that the activation curve is shifted to more depolarized potentials for HCN1 mediated channel populations (Chen at al., 2001; Santoro et al., 2000). It also appears that the kinetics of HCN3 and HCN4 activation are slow compared to HCN1/2 (Ishii et al., 2001; Mistrík et al., 2005; Seifert et al., 1999). It should be noted, however, that HCN1/2 kinetics are generally characterized by time-courses with two exponential components while activation and deactivation currents were fit with single exponential functions for HCN3-4. Experiments in which HCN1 and HCN2 were co-transfected into oocytes indicate that the properties of I_h in these cells cannot be accounted for by linear sums of the two currents, indicating that HCN subunits can form heteromers to produce I_h (Chen et al., 2001). Finally, in line with Difrancesco and Tortora's (1991) hypothesis that cAMP binds directly to channels that mediate I_h, evidence was obtained indicating that there is a binding site for cAMP on the C-terminus of the HCN subunits (Viscomi et al., 2001). Interestingly, whereas cAMP produces large shifts in the voltage dependent activation functions and accelerated kinetics for HCN2 and HCN4 mediated I_h, HCN1 and HCN3 are substantially less sensitive to cAMP (Chen et al., 2001; Mistrík et al., 2005; Viscomi et al., 2001).

1.4 FUNCTIONS OF IH

The variability in the biophysical properties of I_h, resulting in part from molecular diversity of the HCN gene family, coupled with the fact that different HCN subunits and/or subunit combinations are found in different regions of the brain and heart (Santoro & Tibbs, 1999; Robinson & Seigelbaum, 2003), results in a diverse repertoire of I_h functions. One of the most basic functions of I_h in neurons is its influence on the resting membrane potential (V_{rest}) by producing inward current that raises V_{rest}. Further, the conductance resulting from h-channels open at rest reduces the input resistance (R_{in}) and thereby decreases the membrane time constant (τ_m, Pape, 1996). I_h has also been shown to influence the characteristics of synaptic integration and signal transmission from dendrite to soma in pyramidal neurons (Magee 1998, 1999). For instance, in hippocampal and neocortical neurons there is a gradient of I_h expression, increasing from somata to distal apical dendrites (Berger et al., 2001; Magee, 1998). When synaptic inputs depolarize the membrane from rest, the deactivation of the inward current produced by I_h can be interpreted as an effective outward current. The combined effect of this effective outward current and the decreased τ_m resulting from h-channel conductance is that the EPSP decay time-course is more rapid when I_h is present, and this decreases the temporal summation of voltage responses to synaptic input trains (Magee, 1998). The increased density of I_h in distal dendrites renders synaptic decay faster as distance from the soma increases (Magee, 1999), therefore counteracting the time-course attenuation associated with passive signal propagation (Rall, 1977).

There is also a variety of I_h effects on the rhythmic behaviors of cardiac cells and neurons. First, I_h has been shown to support autorhythmicity in both SAN cells and thalamic relay cells. When a SAN cell repolarizes following an action potential, the hyperpolarization results in I_h activation that produces negative feedback and starts to depolarize the cell back towards threshold. This feedback helps to maintain the cardiac rhythm. Similarly, in thalamic neurons, the repolarization following brief bursts of action potentials activates I_h and the resulting inward current helps to bring the cell back towards action potential threshold (Pape, 1996; Robinson & Seigelbaum, 2003). I_h also contributes to the expression of neuronal resonance and in some cases spontaneous subthreshold membrane potential oscillations (Hutcheon & Yarom, 2000). For instance, in EC layer II stellate cells, depolarization to potentials near the action potential threshold results in spontaneous membrane potential oscillations resulting from the opposing effects of I_h and a persistent (non-inactivating) sodium current (I_{NaP}, Dickson et al., 2000). Depolarization of the membrane to potentials between -50 and -60 mV by direct current injection results in an inward current mediated by I_{NaP} activation. The depolarization resulting from I_{NaP} activation deactivates I_h, and thereby this I_h deactivation decreases the depolarizing drive. When I_h is deactivated and the potential starts to move back in the hyperpolarizing direction, I_{NaP} starts to deactivate, I_h is activated again, and the resulting inward current evokes depolarization which then results in I_{NaP} re-activation, thus completing a cycle. This function of I_h is a direct result of the highly depolarized activation function for I_h in these EC stellate cells (Dickson et al., 2000).

I_h dependent resonance is also observed in many cells within the activation range for this current (e.g., Hutcheon & Yarom, 2000). Resonance refers to the property of frequency selectivity in systems that show maximal output responses to inputs at a particular frequency centered within a certain bandwidth. In neurons, resonance is expressed when oscillating inputs at a particular frequency – the resonant frequency – produce voltage responses that are larger than the responses to any inputs at lower or higher frequencies (Hutcheon and Yarom, 2000).

The resonant frequency is the frequency at which the membrane impedance, the frequency domain analog to resistance, is maximal. Neuronal resonance is typically measured by applying sinusoidal currents with a linearly increasing frequency component but constant amplitude (Fig 9A). For low frequency inputs where the time constants of I_h activation and deactivation (τ_h) correspond to h-current "frequencies" higher slower than the voltage response frequency (i.e., $1/2\pi\tau_h < 1/2\pi\tau_m$ and $\tau_h > \tau_m$), I_h attenuates the voltage response. This occurs because the activation of inward I_h during the hyperpolarizing phase of the input decreases the hyperpolarization and deactivation of I_h during the depolarizing phase reduces the amplitude of the depolarizing response due to the effective outward current. At high frequencies the membrane capacitance low-pass filters the input, leaving a frequency window where the impedance becomes maximal at the resonant frequency.

1.5 THE PRESENT STUDY

While the properties and functions of I_h have been characterized in principal neurons from several regions including the thalamus and cortex (e.g., McCormick & Pape, 1990a; Solomon & Nerbonne, 1993a,b), analyses of I_h in inhibitory interneurons is comparatively rare. Biophysical characterizations of interneuronal I_h have only been completed in CA1 stratum oriens cells (Maccaferri & McBain, 1996), CA1 SR/SLM interneurons (Yan et al., 2009), DG fast spiking cells (Aponte et al., 2006), and prefrontal cortex interneurons (Wu & Hablitz, 2005). Because different classes of interneurons have been shown to have distinct functional roles both *in vitro* and *in vivo* (e.g., Klausberger & Somogyi, 2008; Miles et al., 1996; Tamás et al., 2002) and voltage gated channel expression often differs between neurons of separate classes (e.g., Nusser, 2009; Toledo-Rodriguez et al., 2004), specific channels might confer separate physiological characteristics to distinct interneuron classes. It is known that I_h is expressed in SR/SLM interneurons and that this current supports reduced temporal summation of MF-PP inputs activated sequentially (Calixto et al., 2008), but the biophysical properties and effects of I_h on inputs trains resembling *in vivo* activity have not been determined in these neurons.

In this document I provide a detailed biophysical characterization of I_h in SR/SLM interneurons based on the application of curve fitting algorithms to the results of voltage clamp experiments. Given my biophysical assessments, I constructed a novel model of I_h that extends the typical Hodgkin-Huxley models. The model described in this paper simulates I_h with two kinectic components for activation and deactivation, where distinct functions are used to describe both time constant functions of activation and deactivation. Evidence for the functionality of this model is provided based on both simulations and dynamic clamp experiments. Further, a detailed characterization of the model function is presented based on the simulations. Finally, I have assessed the physiological consequences of I_h in SR/SLM interneurons by examining the effects of I_h on temporal summation of input trains and membrane resonance. My results indicate that I_h reduces temporal summation of excitatory input but does not confer resonance within the channel conductance activation range in SR/SLM interneurons. Possible implications of these findings for pattern separation and pattern completion functions of CA3 are discussed.

2.0 METHODS

2.1 SLICE PREPARATION AND RECORDING

Transverse slices of juvenile rat hippocampus were prepared and recordings were made in whole cell configuration from putative interneurons with somata located in either SR or SLM. Sprague-Dawley rats (18-28 days old) were deeply anaesthetized by intraperitoneal administration of Nembutal (5 mg per 100 g body weight). When rendered unresponsive, intracardial perfusions of an ice cold sucrose based solutions were performed. The solution contained (in mM) 210.0 sucrose, 2.8 KCl, 2.0 $MgSO_4$, 1.25 Na_2HPO_4, 25.0 $NaHCO_3$, 10.0 glucose, 1.0 $CaCl_2$, and 1.0 $MgCl_2$ at pH ~ 7.3, maintained by carbogen aeration (95% O_2, 5% CO_2). Vasculature content clearance was complete after 1-2 min of perfusion, after which brains were removed rapidly. Tissue sections containing the hippocampus were glued onto an agar platform, submerged in sucrose solution, and then 300-400 μm slices were obtained using a Leica VT1000S vibrating microtome. The slices contained transverse sections of the hippocampus from approximately the middle third of the structure. Slices were then incubated for 1 hour at 33ºC in a solution containing (in mM) 125.0 NaCl, 2.5 KCl, 1.25 Na_2HPO_4, 25.0 $NaHCO_3$, 10.0 glucose, 1.0 $CaCl_2$, 4.0 $MgCl_2$, and 0.4 ascorbic acid (pH ~ 7.3, 95/5% O_2/CO_2 bubbled in solution). Following the incubation period, the slice chamber was removed from the incubator and slices were left at room temperature for an additional 30 min. For electrophysiological recordings, slices were placed in a submersion recording chamber and superfused with the following solution (in mM): 125.0 NaCl, 2.5 KCl, 1.25 Na_2HPO_4, 25.0 $NaHCO_3$, 10.0 glucose, 2.0 $CaCl_2$, and 2.0 $MgCl_2$ bubbled with carbogen. The temperature of the perfusion bath was maintained at 33ºC with a feedback temperature controller.

The recording chamber was located under a light microscope equipped with differential interference contrast optics and a video camera connected to a monitor. Putative interneurons within SR and SLM were visually selected for recordings. Somata were considered to reside within SR or SLM if they were located >100 µm from *stratum pyramidale* and below the hippocampal fissure (see Fig 1). Whole cell configuration patch clamp recordings were obtained with boroscillate glass pipettes containing (in mM) 120 CH_3KO_4S, 20 KCl, 10 HEPES, 0.5 EGTA, 4.0 NaCl, 4.0 MgATP, 0.3 TrisGTP, 14 phosphocreatine, and 0.2% biocytin or 135 K-gluconate, 10 KCl, 1.0 EGTA, 10 HEPES, 1.0 $MgCl_2$, 2.0 NaATP, and 0.4 NaGTP (pH ~ 7.25). All recordings were made using an Axoclamp-2A amplifier in bridge or voltage clamp mode except the temporal summation experiments, for which an Axopatch-1D was used. Signals were digitized at 10 kHz after being low-pass filtered at 3 kHz. Pipette tip resistances were ~1.5-4.5 MΩ when filled with internal solution and series resistance was ~5-15 MΩ, compensated up to 80% using the amplifier's bridge dial. Data were acquired and in some cases the amplifier's current source and voltage clamp outputs were controlled using the freely available G-Clamp software package (written by Paul Kullmann in LabVIEW, Kullmann et al., 2004). All analyses were completed using custom scripts written in Matlab.

NMDA and $GABA_A$ receptors were blocked with the addition of 50 µM D-2-amino-5-phosphonopentanoic acid (D-AP5) and 10 µM (-)-bicuculline methobromide to the perfusion media in all experiments except the ZAP recordings (see below). For the voltage clamp analyses of I_h, 6-cyano-7-nitroquinoxaline-2,3-dione (CNQX), tetrodotoxin (TTX), and 4-aminopyridine (4-AP) were added to the perfusion bath and I_h was pharmacologically isolated by blocking I_h with ZD7288 (see below). For temporal summation experiments, concentric bipolar electrodes were placed in the suprapyramidal blade of DG (Calixto et al., 2008) and stimulated to evoke MF responses.

2.2 VOLTAGE CLAMP DATA ANALYSIS

I_h was isolated pharmacologically by applying voltage clamp protocols in the absence and presence of ZD7288. Sets of traces were averaged for each protocol (Fig 2A and B, top panels) under baseline and drug conditions and I_h was operationally defined as the difference between the two sets of averaged traces for each protocol, as determined by digital subtraction. The ionic reversal potential for I_h (E_h) was estimated as follows. Neurons were held at -50 mV then a 1.2 s voltage step to -120 mV was applied to activate the channels (Fig 2B). Following channel activation at -120 mV, steps to potentials between -110 and -60 mV were applied and the tail currents were measured immediately following the depolarizing steps from -120 mV (~3 ms). These current values were normalized to the measurements at -100 mV and then averaged across cells. Linear regression over the resulting set of values gave the relation between I_h and the membrane potential for the steady-state h-channel conductance at -120 mV. E_h was estimated algebraically by using the linear fit parameters to find the potential where the extrapolated current was zero. A separate protocol was used to assess the voltage dependence and kinetics of I_h activation: cells were held at -50 mV then hyperpolarized for 1.2 s to potentials between -60 and -120 mV on consecutive iterations of the protocol (Fig 2A). Current measurements at the end of each hyperpolarizing voltage step were divided by driving force for assessment of voltage dependent conductance, $g_h(V) = I_h(V)/(V - E_h)$. Resulting sets of conductance values were normalized to the conductance at -120 mV and averaged across neurons. The resulting data set was fitted with the following equation to describe the normalized steady state voltage dependence of I_h activation (X_∞):

$$X_\infty(V) = g_h(V) / g_h(-120 \text{ mV}) = A / (1 + \exp[(V - V_{1/2}) / k]) + (1 - A) \qquad (\textit{Eq. 1})$$

where A is the voltage dependent component of the fractional conductance ($0 < A < 1$), $1 - A$ is a voltage independent component, $V_{1/2}$ is the voltage at half-maximal activation, and k is a slope parameter. For this (*Eq. 1*) and other curve fits, the fit quality was evaluated by assessment of goodness of fit statistics. R^2 values were computed in order to determine how well the models explained the fitted data sets ($0 < R^2 < 1$). Higher R^2 values were taken to indicate statistically superior fits. The voltage dependent kinetic properties of I_h were assessed by fitting exponential curves to ZD7288 sensitive traces where I_h was either activating (Fig 2A, Fig 3A) or deactivating (Figs 2B and 3B). The following equations were used to fit the I_h activation and deactivation traces at each voltage step, respectively, with two exponential time constants:

$$I_A(t) = I_{A,f}\,(1 - \exp(-t / \tau_{A,f})) + I_{A,s}(1 - \exp(-t / \tau_{A,s})\,) \qquad (\textit{Eq. 2})$$

$$I_D(t) = I_{D,f}\exp(-t / \tau_{D,f}) + I_{D,s}\exp(-t / \tau_{D,s}) \qquad (\textit{Eq. 3})$$

where A and D denote activation and deactivation, f and s are for fast and slow current (I) components and corresponding time constants (τ). The curves were also fitted with single exponential curves (i.e., by setting $I_{A,f}$ and $I_{D,f}$ to zero), however, the double exponential fits were superior in all but a few rare cases, based on R^2 and *p* values for F-statistics.

2.3 COMPUTATIONAL MODELING

I constructed a modified Hodgkin-Huxley (HH) type mathematical model (Hodgkin & Huxley, 1952) of I_h based on curve fits applied to our voltage clamp data (see below, Figs 2 and 3). While the available HH-type models of I_h only incorporate one or two equations for the voltage dependent channel kinetics, our results, along with similar findings from other laboratories, suggest that these models may be inconsistent with experimental data. This inconsistency results from (a) the fact that I_h deactivation is often found to be faster than activation at a given potential (Fig 3C,D; e.g., Magee, 1998;), and (b) both I_h activation and deactivation kinetics are often described optimally by double rather than single exponential fits (Fig 3; e.g., Solomon & Nerbonne, 1993b). I expanded the previous convention for modeling I_h based on the HH formalism to incorporate the results from our experiments and curve fits. In order to verify the functionality of this I_h model, I implemented a single compartment neuron model with I_h. The model consisted of membrane capacitance (C_m), a voltage independent "leak" conductance (g_L), and the h-conductance (g_h), all in parallel. Current pulses and synaptic conductances were applied to the model and the voltage across C_m was computed according to the current balance equation:

$$C_m\,(dV/dt) = -(I_L + I_h) + I_{ext} \qquad (Eq.\ 4)$$

Here I_{ext} is an externally applied current, $I_L = g_L(V - E_L)$ is the leak current, E_L is the leak reversal potential, and I_h is the h-current described in detail below (see Results). The neuron was modeled as spherical unit with a diameter of 40 μm. Specific parameters for passive model properties were chosen to be C_m = 1.0 μF/cm^2 (e.g., see Carnevale et al., 1997; Spruston & Johnston, 1992) and g_L = 0.04 mS/cm^2 so that the passive membrane time constant was τ_m =

C_m/g_L = 25 ms, E_L = -75 mV, and the resulting resting membrane potential was -70 mV when I_h was present. These parameter choices yield values of V_{rest} and τ_m consistent with previous measurements from SR/SLM interneurons (Anderson et al., 2008; Calixto et al., 2008). Simulations were completed using Matlab where *Eq. 4* was solved using forward Euler integration, as in dynamic clamp experiments, with a time step of dt = 100 μs corresponding to the 10 kHz sampling frequency used in experiments. The use of faster time step values (e.g., dt = dt = 10 μs) did not alter the results of my simulations.

2.4 DYNAMIC CLAMP

The functionality of my I_h model was assessed using dynamic clamp simulations of the model during recordings from SR/SLM interneurons. The dynamic clamp recording configuration allows for effectively applying the voltage- and time-dependent current that would go through a population of voltage gated channels according to a mathematical formulation of the conductance's time and/or voltage dependent properties. This is accomplished by interfacing a recording amplifier with a computer that performs real time computations at each sampling interval in order to send a current value to the current command terminal of the amplifier so that this current can be applied to a cell. I used a dynamic clamp configuration based on a system originally described by Kullmann and colleagues (2004).

The hardware for this system consists of the Axoclamp-2A amplifier, a desktop computer running Windows XP, a 16 bit data acquisition (DAQ) board, and a PC running a real-time operating system (National Instruments). The desktop PC, referred to as the "host computer," has the LabVIEW development system and G-Clamp software installed. The other computer running a real-time operating system, referred to as the “embedded PC,” is equipped with the LabVIEW development system and the LabVIEW Real-Time Module (see Kullmann et al., 2004 for details). Dynamic clamp of a given conductance, g_s, is accomplished by this system as follows. The amplifier is set to bridge mode and measurements of the membrane potential are relayed to the DAQ board, which digitizes the potential at each time interval. The DAQ board relays potential values to the embedded PC, at which point the value of g_s is computed based on the time and the potential at the given time point, according to a specified mathematical model. The current (I_s) that would pass through a population of s-channels is then computed, $I_s = -g_{s,max} X(V - E_s)$ where X is the activation fraction, and this value is relayed back to the amplifier via the DAQ board. The negative sign in the previous equation is there because, for instance, the amplifier needs to apply positive (depolarizing) charge for $V < E_s$ in order to simulate g_s. When the amplifier applies I_s to the cell, the current command resembles the current through a population of s-channels, and g_s is therefore artificially induced. At every sampling interval, the embedded controller save the values of V and I_s and send this data back to the host after the dynamic clamp protocol is completed.

The dynamic clamp functions of the embedded controller are controlled by G-Glamp, which is running on the host PC. The mathematical characterization of I_h was programmed into G-Clamp and various parameters for individual dynamic clamp protocols (e.g., sampling frequency, time span, current step magnitudes, $g_{h,max}$, etc.) are set in G-Clamp and then downloaded onto the controller. The controller executes the protocols that are parameterized in G-Clamp when the user prompts the software to execute the given protocol, and when completed, sends the V and I_h data back to the host for presentation in G-Clamp and storage on the hard disk.

2.5 ZAP STIMULUS AND ANALYSIS

I tested the hypothesis that I_h imparts subthreshold membrane resonance to SR/SLM interneurons by applying sinusoidal current inputs with a linearly increasing frequency and constant amplitude (i.e., a ZAP stimulus, see Fig 9A, Puil et al., 1986). This input was generated by applying a current command according to the following equation:

$$I_{ZAP}(t) = A \sin(at^2 + bt) \qquad (Eq.\ 5)$$

For this expression, A is the amplitude of the stimulus, $a = (\omega_2 - \omega_1)/2T$, and $b = \omega_1$ where T is the total time of the waveform, $\omega_i = 2\pi f_i$, f_1 = the initial frequency, and f_2 = the final frequency. Values of 0 Hz and 15 Hz were used for f_1 and f_2, respectively, and A was selected so that the upward voltage deflections were between 5 and 10 mV. The impedance as a function of frequency is $Z(f) = R + jX$ where R = resistance, X = reactance, and $j = (-1)^{1/2}$. The impedance magnitude $|Z|(f) = (R^2 + X^2)^{1/2}$ was found by using the fast Fourier transform (FFT) algorithm. The magnitude of the FFT of the voltage response divided by the FFT of I_{ZAP} to get the impedance magnitude $|Z|(f) = |FFT(V)/FFT(I_{ZAP}(t)|$. These computations were used for plots of impedance as a function of input frequency, yielding impedance amplitude profiles (ZAPs, Puil et al., 1986). The noisy impedance traces were smoothed using cubic spline interpolation for assessments of peak impedance values (Fig 9).

3.0 RESULTS

3.1 BIOPHYSICAL PROPERTIES OF IH IN SR/SLM INTERNEURONS

Roughly 50% of the neurons found in either SLM or SR displayed a membrane potential “sag” following hyperpolarization in current clamp, indicative of I_h activation. I applied either one or both voltage clamp protocols illustrated in figure 2 (A and B, top) in the presence and absence of 50 μM ZD7288 to 16 putative interneurons located in SLM or SR. Sets of traces were averaged then digitally subtracted and the resulting ZD7288 sensitive traces were used for all analyses of I_h described below. All experiments were completed in the presence of 50 μm AP5, 10 μm CNQX, 10 μm bicuculine, 3 mM 4-AP, and 1 μm TTX.

3.1.1. *Reversal Potential and Voltage Dependence of I_h Activation*

To estimate the net reversal potential for the ionic current mediating I_h, we applied 1.2 s voltage steps from -50 mV to -120 mV to activate the channels before depolarizing the neurons to potentials between -110 and -60 mV (Fig 2B). Tail currents were measured in order to obtain the currents for a given conductance over a range of driving force values. The normalized current values were averaged and plotted as a function of step potential (resulting averaged values were multiplied by -1 for presentation). A linear fit was applied to the resulting data set and E_h was estimated via extrapolation as the intercept of the linear fit with the abscissa (Fig 2C). Consistent with reported measurements, E_h was estimated to be -33.7 mV in SLM/SR interneurons (n = 9) resulting from the channel selectivity for both Na^+ and K^+ ions. This value of E_h was then used to determine h-channel conductance, g_h. To determine the voltage dependence of g_h activation, currents were measured right before the terminations of hyperpolarizing pulses from -50 mV to potentials between -60 and -120 mV. The currents measured at each potential were divided by the respective driving force to determine the conductance at that potential. Resulting values were normalized and averaged across neurons (n = 11). A sigmoidal curve with both voltage dependent and voltage independent components was fit to the averaged normalized

values (*Eq. 1*, Fig 2D). This fit was superior to an equation applied to the data without a voltage independent component (i.e., A = 1) based on R^2 values for the models. Model parameters obtained were as follows: A = 0.92, $V_{1/2}$ = -88. 8 mV, and k = 10.0 mV. Assessments of E_h and $g_{h,max}$ were made for each cell and summary results are presented in Table 1.

Table 1. *Summary: biophysical properties of I_h in SLM/SR interneurons.*

	Mean	SEM	N
E_h (mV)	-31.5	6.24	9
g_h(-120 mV) (nS)	2.6	0.30	11
A	0.90	0.034	11
$V_{1/2}$ (mV)	-89.4	1.41	11
k (mV)	9.22	0.40	11

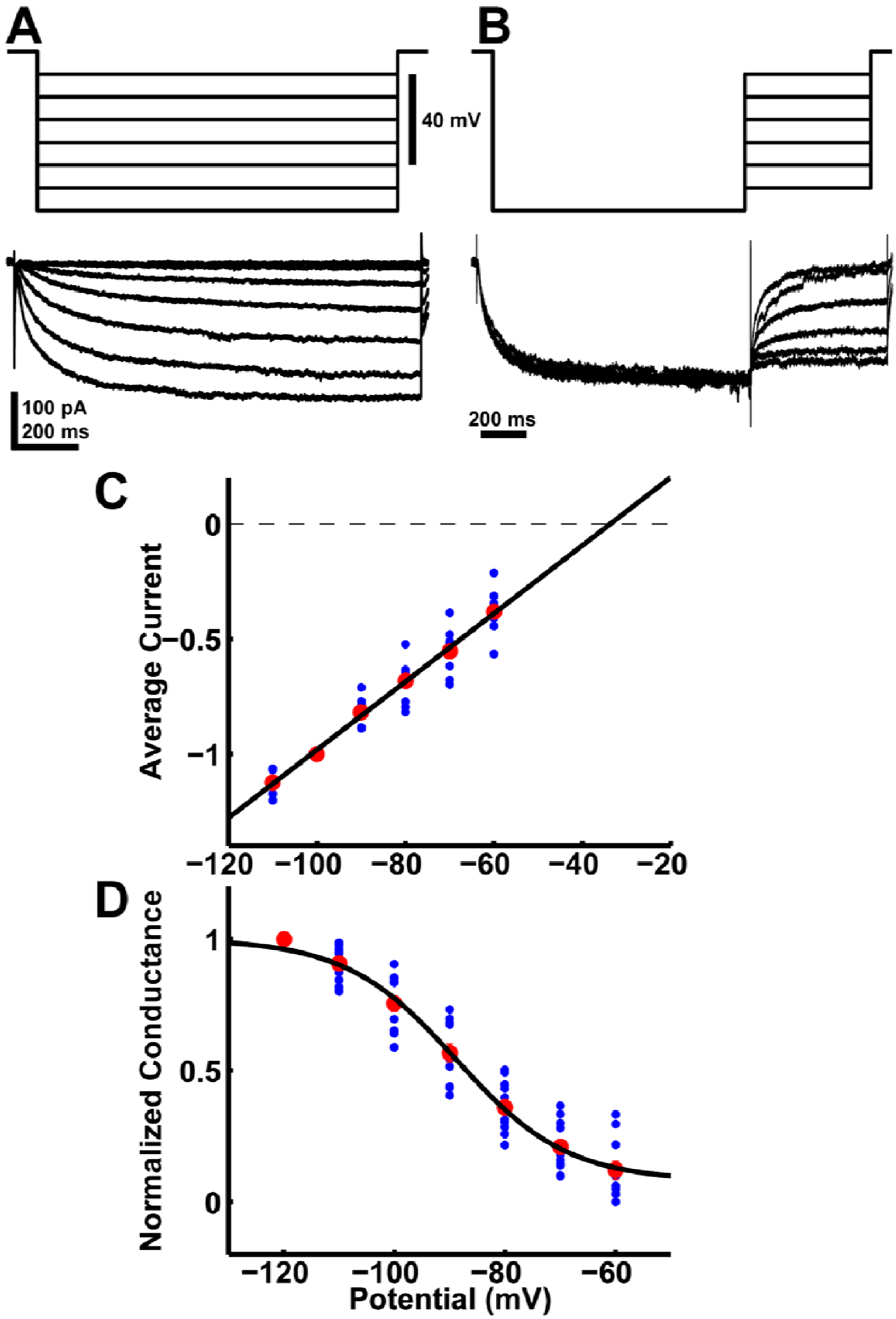

Figure 2. *Voltage dependence and reversal potential of I_h.* **A and B:** The top panels of **A** and **B** show schematics of the voltage clamp protocols applied. The lower panels show the resulting ZD7288 sensitive currents evoked from the execution of these protocols. **C:** To estimate E_h, the current was measured in **B** right after the steps from -120 mV. The individual sets of values were normalized to the value at -100 mV and plotted in blue for each cell (n = 9). A linear fit was applied to the set of value averaged at each potential (red dots with error bars representing ± SEM) and E_h was taken as the voltage at the point where the fit was extrapolated to zero (black trace, E_h = -33.7 mV). **D:** I_h was measured at a time point right before each voltage step was terminated in **A** and these current values were divided by the driving force for each voltage step to obtain conductance. Values were normalized to the conductance at -120 mV and plotted in blue for each cell. These values were averaged across cells (n = 11) for each voltage step and the resulting set (red dots) was fitted with the sigmoid given by *Eq. 1* (black trace).

3.1.2. *Activation and Deactivation Kinetics*

Dual component exponential fits (*Eqs. 2 and 3*) were applied to current traces where I_h was either activated at potentials between -60 and -120 mV (Fig 3A, n = 16) or deactivated at potentials between -110 and -60 mV following a step to -120 mV (Fig 3B, n = 11). When I_h was activated with hyperpolarizing pulses to -120 mV, the fast and slow time constants were 31 ms and 257 ms on average, respectively. Lower magnitude hyperpolarizations resulted in slower activation time constants (Fig 3C & D, red points), consistent with previous findings indicating that I_h activation kinetics increase in speed as a function of hyperpolarization. The fractional contributions from the fast components of I_h activation, $I_{A,f}$ / ($I_{A,f}$ + $I_{A,s}$), increased from 0.49 to 0.64 between -60 and -120 mV (Fig 3E, red), indicating that the fast component of I_h activation contributes ≥ 49% to I_h. As observed previously, deactivation kinetics were faster than activation kinetics (Fig 3C & D, green points; e.g., Magee, 1998). At -80 mV for example, average values for the fast and slow activation time constants were 67 and 601 ms, whereas the fast and slow deactivation time constants were 13 and 141 ms. The fractional contributions of fast deactivation ($I_{D,f}$ / ($I_{D,f}$ + $I_{D,s}$)) were ~0.45 – 0.50 between -90 and -70 mV, and then there was an increase to 0.62 at -60 mV (Fig 3E, green). Hence, the fast component of I_h deactivation is prominent above V_{rest}.

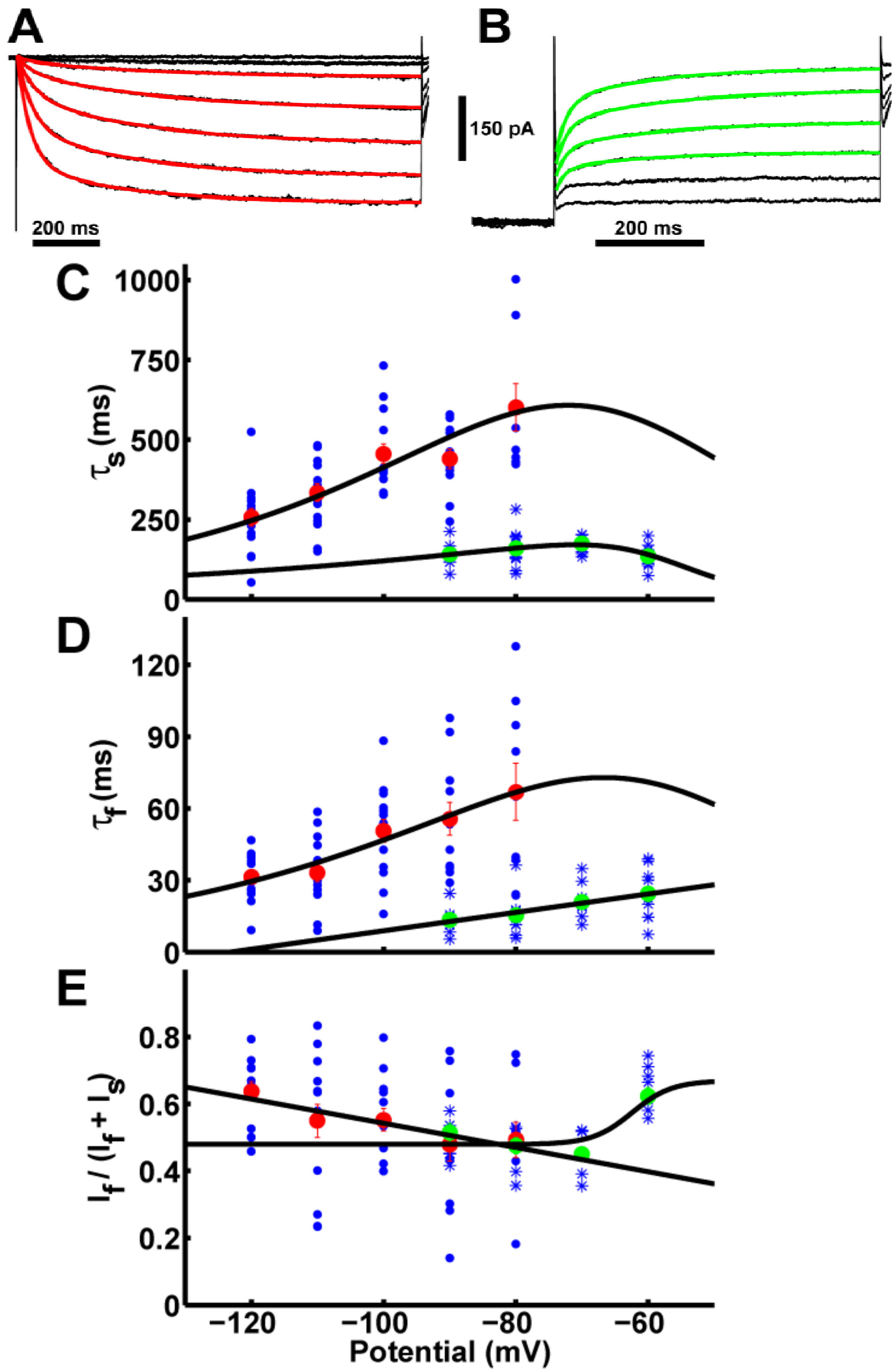

Figure 3. *Activation and deactivation kinetics for I_h.* **A and B:** the same traces from Fig 2A,B are shown with kinetic fits overlaid. For **A**, Eq. 2 was applied at each potential (red) and Eq. 3 was applied to current traces in **B** (green). **C:** The slow time constants of I_h activation ($\tau_{A,s}$) and deactivation ($\tau_{D,s}$) are plotted for each cell (n = 16) in blue dots and blue asterisks, respectively. Average values (red for activation, green for deactivation) were fitted with Eq. 10 (black traces). **D:** Values of the fast time constants of activation ($\tau_{A,f}$) and deactivation ($\tau_{D,f}$) are shown for individual cells in blue while values averaged across cells appear in red and green. Eq. 10 was used to fit $\tau_{A,f}$ and a linear fit was applied to $\tau_{D,f}$. **E:** The fractional contribution of the fast component is plotted for activation and deactivation. *Eqs. 11-13* were fitted to sets of values averaged across cells.

3.2 MATHEMATICAL MODELING OF IH: SIMULATIONS AND DYNAMIC CLAMP EXPERIMENTS

3.2.1. *Mathematical Model*

I_h is typically modeled with the following system of equations:

$$I_h = g_{h,max} X (V - E_h) \qquad (Eq.\ 6)$$

$$\tau_h (dX / dt) = X_\infty(V) - X \qquad (Eq.\ 7)$$

in which $g_{h,max}$ is the maximal conductance for the modeled h-channel population, X_∞ is the normalized steady state level of activation as a function of voltage ($0 < X_\infty < 1$, see *Eq. 1*, Fig2D), and X is a gating variable ($0 < X < 1$) that relaxes towards X_∞ with time constant τ_h. However, this formalism is inadequate for modeling I_h based on my voltage clamp measurements of I_h in SLM/SR interneurons, because (a) the net h-current activates with kinetics slower than for deactivation and (b) the activation and deactivation kinetic fits have two exponential components (*Eqs. 2,3*).

I developed a phenomenological model of I_h that extends the model described by *Eqs. 6 and 7* based on my measurements to accommodate the results of my kinetic fits. Because activation and deactivation kinetics are modeled with separate expressions (see below), the h-current was computed at each time step (dt) with one of two expressions, depending on whether the channel population was determined to be activating or deactivating, respectively:

$$I_{h,A} = g_{h,max} (X_f F_{A,f} + X_s (1 - F_{A,f})) (V - E_h) \qquad (Eq.\ 8)$$

$$I_{h,D} = g_{h,max} (X_f F_{D,f} + X_s (1 - F_{D,f})) (V - E_h) \qquad (Eq.\ 9)$$

where X_f and X_s are fast and slow activation variables, $F_{A,f} = I_{A,f} / (I_{A,f} + I_{A,s})$ and $F_{D,f} = I_{D,f} / (I_{D,f} + I_{D,s})$ are voltage dependent functions (see below) describing the fractional contributions of fast activation and deactivation (Fig 3E), and other terms are as described previously. Hence, $I_h(t) = I_{h,A}(t)$ or $I_{h,D}(t)$. In this formulation, activated I_h is the sum of fast and slow components, $I_h = I_{h,f} + I_{h,s}$ where $I_{h,f} = g_{h,max} X_f F_{A,f} (V - E_h)$ is the fast component and $I_{h,s} = g_{h,max} X_s (1 - F_{A,f}) (V - E_h)$ is the slow component of I_h activation. Analogous reasoning applies for I_h deactivation. To determine whether the channels were activating or deactivating, the fractional conductance (X) was compared to the normalized steady state conductance (X_∞) at each time step (see also Appendix A). The fractional conductance of I_h is either $X(t) = (X_f(t) F_{A,f}(t) + X_s(t) (1 - F_{A,f}(t)))$ if I_h is activating at time t or $X(t) = (X_f(t) F_{D,f}(t) + X_s(t) (1 - F_{D,f}(t)))$ if I_h is deactivating.

In order to determine whether I_h was activating or deactivating at time t, $X(t - dt)$ was compared to $X_\infty(V(t))$ and the following logic was applied in simulations at each time step:

IF $\quad$ $X(t - dt) \leq X_\infty(t)$, then I_h is activating

ELSE $\quad$ I_h is deactivating

Eq. 8 was used when I_h was activating and *Eq. 9* was used when I_h was deactivating (see Fig 4C,D). If I_h was determined to be activating at a given time step, the gating variables (X_f and X_s) were updated using the activation time constants, and X(t) and $I_h(t)$ were computed using the updated gating variables and the activation fractional components. For $X(t - dt) > X_\infty(t)$, I_h was considered to be deactivating and the corresponding deactivation time constants were used to update the gating variables (See Appendix A). The equations describing the gating variables were solved with the Euler method:

$X_i(t) = X_i(t - dt) + (dt / \tau_{j,i}(V)) (X_\infty(V) - X_i(t - dt)),$ (*Eq. 10*)

in which i designates either f or s and j stands for A or D. The algorithm for computing I_h is portrayed in a "pseudo-code" in Appendix A.

The voltage dependent functions used to describe the kinetic parameters were based on curve fits to averaged data points in figure 3 (panels C and D). The following equation was used for $\tau_{A,s}$, $\tau_{D,s}$, and $\tau_{A,f}$:

$\tau_{j,i}(V) = x / (a \exp[V / k_1] + b \exp[-V / k_2]), i = f,s; j = A,D$ (*Eq. 11*)

For $\tau_{A,s}$, the parameter set was {x = 122.1, a = 1.955, b = 0.01528, k_1 = 22.45, k_2 = 34.69}, for $\tau_{D,s}$, {x = 30, a = 320.2, b = 0.05197, k_1 = 7.243, k_2 = 63.85}, and for $\tau_{A,f}$ the fit parameters were {x = 129.5, a = 12.93, b = 0.2166, k_1 = 22.09, k_2 = 40.07}. A linear fit was used for the fast deactivation time constant, $\tau_{D,f}(V) = aV + b$, with a = 0.3843 and b = 47.34 (see black curves in Fig 3C,D). The fractional contributions of the fast current components (Fig 3E) were described by the following equations:

$F_{A,f}(V) = I_{A,f} / (I_{A,f} + I_{A,s})(V) = aV + b$ (*Eq. 12*)

$F_{D,f}(V) = I_{D,f} / (I_{D,f} + I_{D,s})(V) = p + x / (1 + \exp[(V_x - V) / k])$ (*Eq. 13*)

The resulting parameter sets were {a = -0.003614, b = 0.1807} for $F_{A,f}$ and {p = 0.479, x = 0.19, V_x = -62.4, k = 3} for $F_{D,f}$ (see black curves in Fig 3E).

3.2.2. *Simulations*

This model for I_h was implemented in a resistor-capacitor circuit model described above (see Methods). Comparisons were made with simulation results in a model cell without I_h where V_{rest} was set at -70 mV by changing E_L from -75 to -70 mV; all other parameters were the same. When 500 ms hyperpolarizing current square steps were applied to the model neurons (I_{ext} = -2

mA/cm^2), the neuron with I_h showed the typical membrane potential “sag” during hyperpolarization whereas the neuron without I_h had a larger input resistance and no sag (Fig 4A). As the membrane hyperpolarizes during the negative current step, I_h activation resulted in increasingly negative (inward) h-current (Fig 4B, downward deflection). In contrast, during depolarization resulting from positive current injection (I_{ext} = 1 mA / cm^2), the deactivation of I_h resulted in less inward current, or the effective outward current mediated by deactivation of the conductance (Fig 4B, upward deflection).

To examine the behavior of I_h in more detail, various model parameters were plotted over time (Fig 4). When the model neuron received positive direct current input (Fig 4A), X_∞ was reduced during the pulse and the normalized steady state conductance X followed X_∞ (Fig 4C, top). Because X was greater than X_∞ while the depolarizing input was being applied, I_h was equal to $I_{h,D}$ during the depolarization (Fig 4C, bottom, green segment of the trace). When the current square step was terminated, X_∞ began to increase as the membrane potential relaxed back to V_{rest}. Because X was less than X_∞ during this phase of the simulation, I_h was equal to $I_{h,A}$ and I_h activation increased the amount of inward h-current back to the resting level (red segment). When hyperpolarizing input was applied to the model neuron with I_h (Fig 4A), the membrane potential hyperpolarization increased X_∞ with a corresponding increase in the X (Fig 4D, top). Because X was less than X_∞ during the hyperpolarization, I_h was equal to $I_{h,A}$ as activation increased (Fig 4D bottom, red segment). When the hyperpolarizing pulse was terminated and V relaxed back to V_{rest}, X_∞ returned to the resting level faster than X, and I_h was equal to $I_{h,D}$ during the deactivation of the conductance (green segment). The smooth evolution of the activation variables is shown for depolarizing and hyperpolarizing inputs in panels E and F of figure 4, respectively.

Simulated excitatory input was also applied to the model in place of I_{ext} (Fig 4G,H). The waveform for an excitatory synaptic conductance was given by $g(t) = \exp(-t/\tau_d) - \exp(-t/\tau_r)$ where τ_r and τ_d are the synaptic rise and decay time constants, respectively. The normalized conductance waveform was $g_{wave}(t) = g(t)/g(t_{peak})$ where $g(t_{peak})$ is a scaling factor given $t_{peak} = [\tau_d\ \tau_r / (\tau_r - \tau_d)]\ \mathrm{Log}_e(\tau_r / \tau_d)$. The synaptic conductance (termed $g_{syn}(t)$) for a simulated train of 5 inputs was simulated at 50 Hz. The synaptic conductance input $g_{syn}(t)$ was created by convolving $g_{wave}(t)$ with an input timing vector with ones at spike times and zeros elsewhere (Fig 4G, bottom). Synaptic current was computed as $I_{syn}(t) = g_{syn,max}\ g_{syn}(t)\ (V(t) - E_{syn})$ where $g_{syn,max}$ is the amplitude of the synaptic conductance and E_{syn} is the synaptic reversal potential. I_{ext} was replaced by I_{syn} in *Eq. 4*, the synaptic input parameter set was $\{g_{syn,max} = 2.2$ pS, $\tau_r = 0.5$ ms, $\tau_d = 4$ ms, $E_{syn} = 0$ mV$\}$ for these simulations, and all other parameter values were the same as for other simulations of the neurons with and without I_h. As in experiments (e.g., Magee, 1998, 1999, see Fig 6), the presence of I_h resulted in less EPSP summation during an input train (compare red and black traces in Fig 4G). The depolarization resulting from the synaptic conductance inputs deactivated I_h (Fig 4H) which created the effective outward current (i.e., reduction of inward current) that reduced temporal summation of the EPSP response in combination with the effect of increasing R_{in} by taking the h-conductance out of the model.

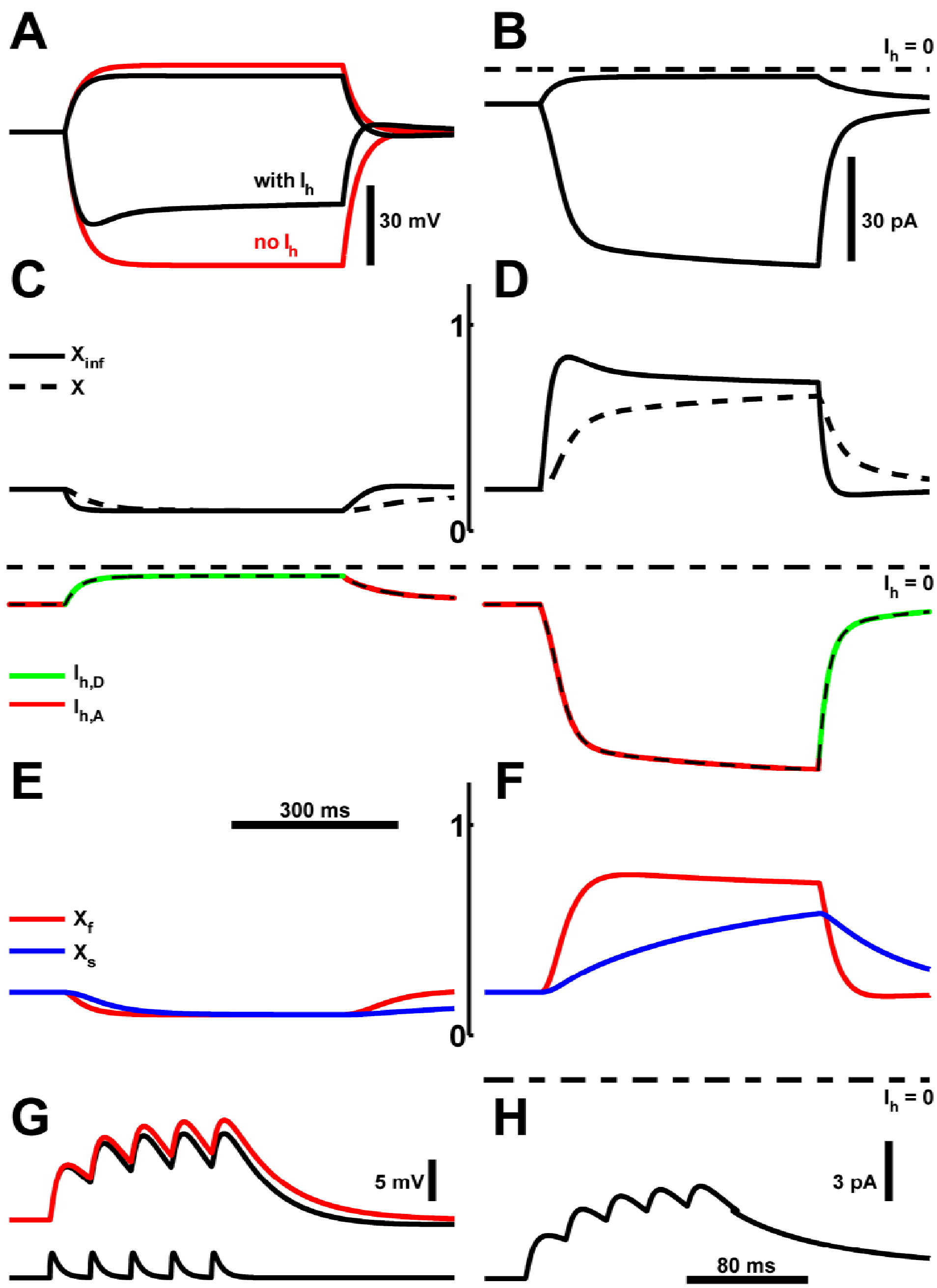

Figure 4. *Mathematical model of I_h.* Simulations were implemented where the neuron was stimulated with current steps in the presence or absence of I_h. When I_h was present, $g_{h,max}$ = 0.027 mS/cm^2 and E_L = -75 mV. In contrast, when I_h was absent E_L = -70 mV so that V_{rest} was -70 mV in both cases. **A:** A hyperpolarizing pulse (-2 mA/cm^2) produced membrane potential sag in the simulation with I_h. **B:** The h-current is plotted over time for both depolarizing (top trace) and hyperpolarizing (lower trace) current steps. When the simulated neuron is depolarizing, the upward deflection of I_h reflects the reduction of the inward current. Hyperpolarizing input results in increased I_h activation and an increase in inward current. **C,D (top):** X_∞ (solid trace, designated X_{inf}) and X (dashes) are plotted for the depolarizing (C) and hyperpolarizing (D) inputs. **C,D (bottom):** I_h is plotted (dashed line) for depolarizing (C) and hyperpolarizing (D) responses; compare with panel B. These traces are plotted over $I_{h,A}$ (red) and $I_{h,D}$ (green, see *Eqs. 8 and 9*) in order to show that $I_h = I_{h,A}$ when $X \le X_\infty$ and $I_h = I_{h,D}$ for $X > X_\infty$. **E,F:** These plots show the smooth evolution of the gating variables during the depolarizing ((E) and hyperpolarizing (F) responses. **G:** Voltage responses (top) to 50 Hz conductance input trains (bottom) are shown when I_h is present (black) or absent (red). **H:** This trace show I_h during the voltage response. The upward deflection indicates that I_h is deactivating.

Additional simulations were completed in order to show the correspondence between model I_h and native I_h. First, I simulated voltage clamp control of the modeled I_h by applying voltage step protocols to the model neuron and computing I_h according to the procedure described above. Model parameters for all simulations were the same as those for the simulations represented by figure 4. As shown in figure 5, the model qualitatively replicates the time-courses of I_h activation and deactivation shown in experimental traces.

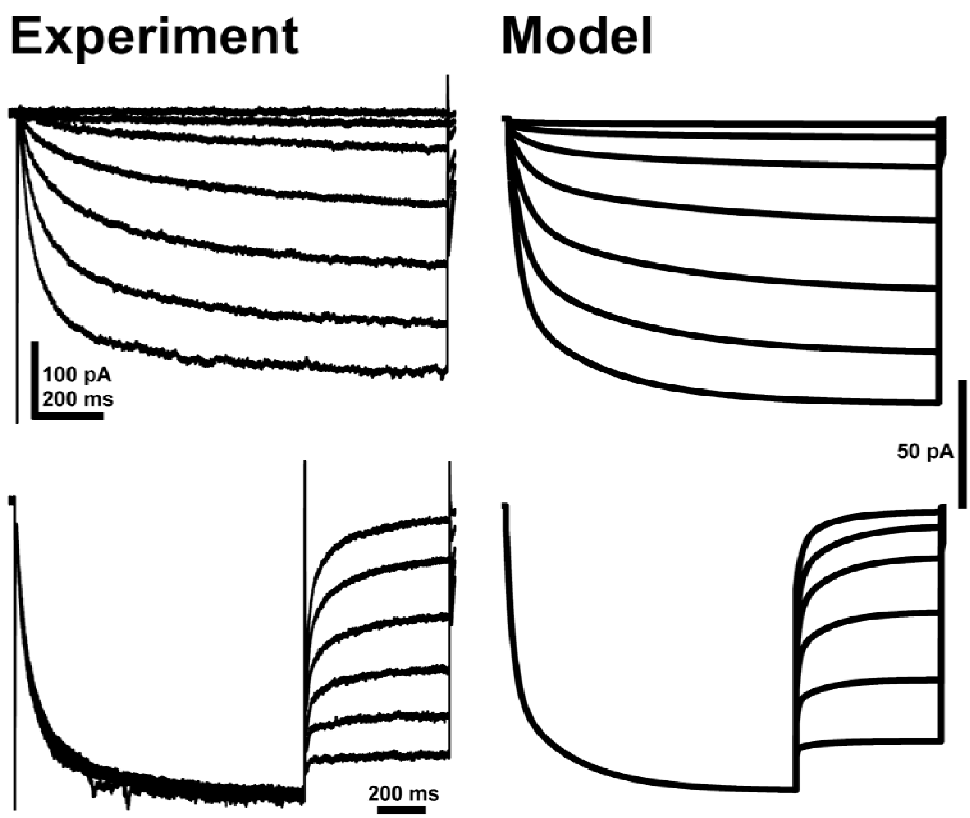

Figure 5. *Comparing model I_h with neuronal I_h in voltage clamp.* The experimental traces (left) are the same as those shown in figure 2 (panels A and B). The traces obtained for the model resemble the experimental traces with respect to the time-courses of I_h activation and deactivation.

In addition to the voltage clamp comparison, I also directly compared the performance of the model with results from an interneuron recording in current clamp (Fig 6). The results show that the I_h model qualitatively replicates both membrane potential sag following hyperpolarization and reduction in temporal summation of 50 Hz input. These results demonstrate the effectiveness of the model in generating the signature features of I_h in both voltage clamp and current clamp simulations.

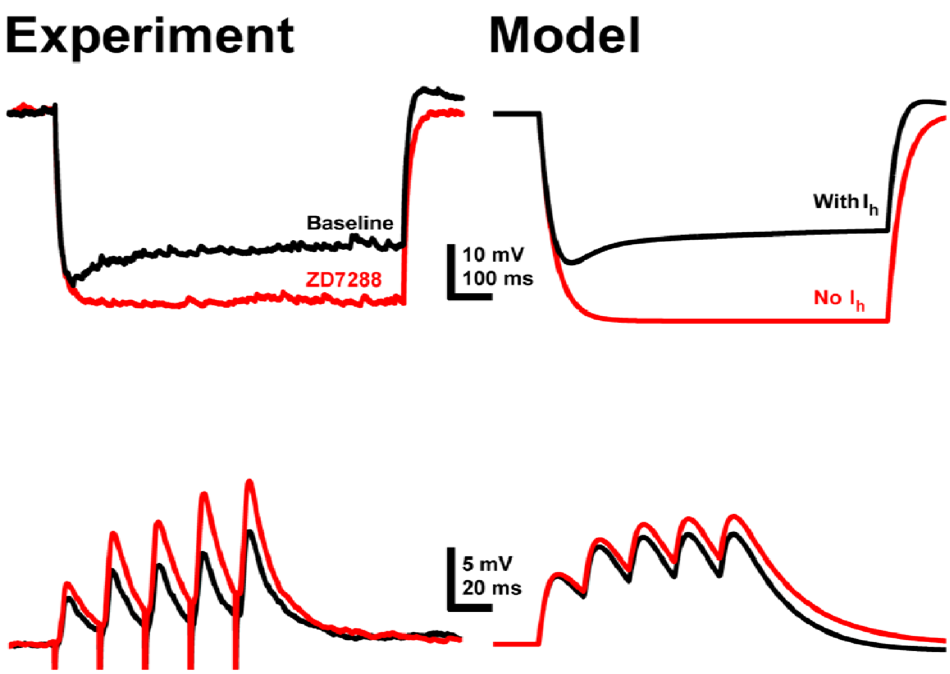

Figure 6. *Comparing model I_h with neuronal I_h in current clamp.* The experimental traces (left) show responses to hyperpolarizing current steps (top) and 50 Hz stimulation of the MF pathway (bottom) with and without pharmacological blockade of I_h. The model responses indicate a comparable effect of the model I_h on summation. The temporal summation traces are the same as those shown in figure 4 while the current step for the top right traces was -1.5 mA/cm^2 for this figure. All other parameters were the same.

3.2.3. *Dynamic Clamp*

The functionality of this model was further examined in dynamic clamp experiments (Fig. 5), where a slightly different version of the I_h model presented above was used which yields qualitatively comparable results to the model presented above. The only difference was that when X(t – dt) was compared to $X_\infty(t)$, $F_{A,f}$ was always used. This makes negligible differences in membrane potential responses because there is not a very big difference between $F_{A,f}$ and $F_{D,f}$, especially at potentials below -60 mV. When I_h is removed artificially be setting $g_{h,max}$ to -0.5 nS in the dynamic clamp code, the sag in the membrane potential response to hyperpolarizing current square steps was abolished (Fig 7, top left). This resulted by adding the time dependent hyperpolarizing current during the current step in order to counteract the effect of the current from endogenous h-channels (Fig 7, bottom left). In contrast, when I_h is added via dynamic clamp to an interneuron without sag ($g_{h,max}$ = 2.5 nS), the current generated by the dynamic clamp command (Fig 7, bottom right) generated membrane potential sag (Fig 7, top right). These results indicate that my novel model captures the signature features of native I_h in SR/SLM interneurons.

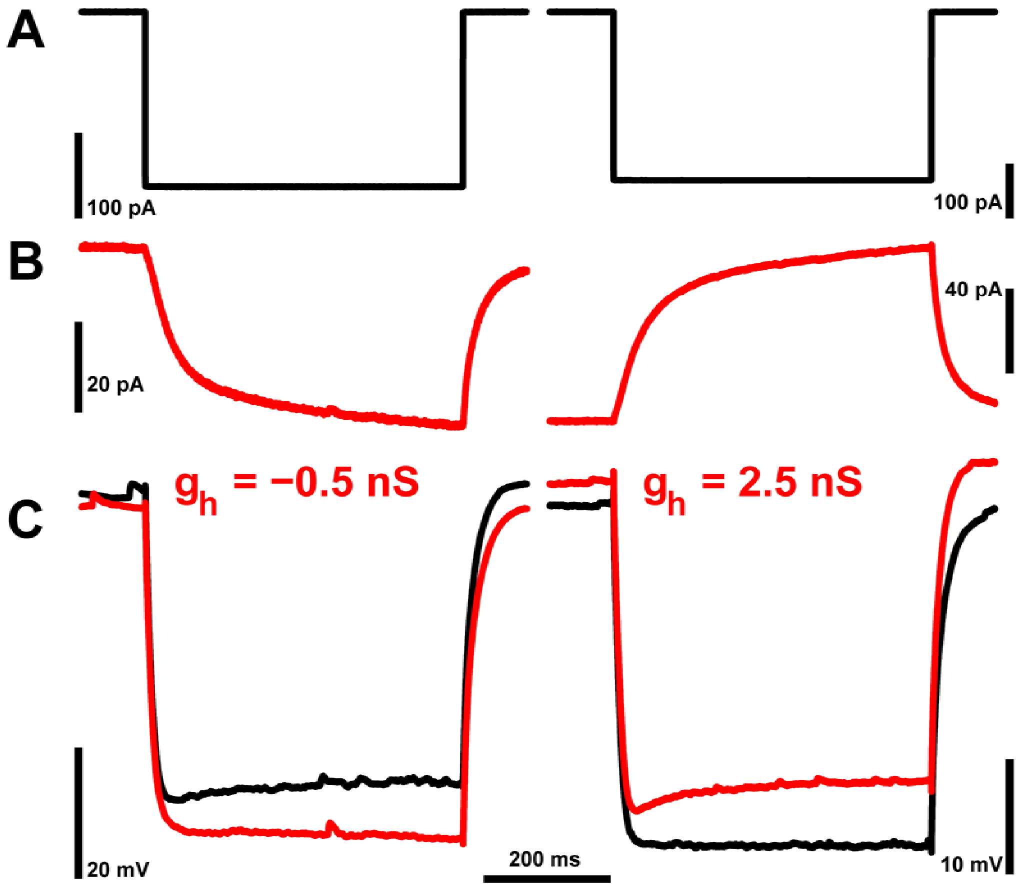

Figure 7. *Dynamic Clamp of I_h.* Our dynamic clamp configuration was used to either electrically "block" (left) or "add" (right) I_h to SR/SLM neurons based on my mathematical model. **A:** Hyperpolarizing current square steps applied to two neurons. **B:** For a cell with I_h (left), the dynamic clamp mediated application of a negative h-conductance ($g_{h,max}$ = -0.5 nS) resulted in the addition of the hyperpolarizing current shown by the red trace during the hyperpolarizing voltage response. In contrast, the dynamic clamp was also used to artificially add I_h to a cell without sag (right). This resulted in the depolarizing current shown by the red trace on the right given $g_{h,max}$ = 2.5 nS. **C:** The voltage responses under baseline conditions (black) and during dynamic clamp of I_h (red) during the hyperpolarizing responses are shown. Adding the negative h-conductance effectively blocked the expression of sag and increased the apparent R_{in} as a result of the increased hyperpolarizing current generated by the dynamic clamp circuit (B, left). The panel on the right shows the effect of electronically adding I_h to a neuron without sag (black trace). When positive h-conductance is added (B, right), the membrane potential sag becomes apparent due to depolarizing current waveform.

3.3 FUNCTIONS OF IH: TEMPORAL SUMMATION AND RESONANCE

3.3.1. *Temporal Summation Experiments*

As shown above, a typical function of I_h is to reduce temporal summation of excitatory synaptic input trains (Fig 6; see Magee, 1998), Mechanistically, the I_h mediated reduction of temporal summation is primarily a result of the fact that when I_h is active at rest, the conductance resulting from activated h-channels decreases τ_m. The increased τ_m in the absence of I_h results in a decrease of the synaptic decay time constant under I_h blockade. For successively activated inputs, less decay of each voltage response to synapse activation occurs when I_h is blocked. The effect of the reduction in the kinetics of synaptic decay is that the voltage response to each input is initiated at a more depolarized potential, and hence, the percent increase in the response amplitude from the first to the last EPSP is greater under I_h blockade when the initial responses are of approximately the same amplitude. Furthermore, because any h-current active at V_{rest} is deactivated during the time-course of a synaptic input train, the inward current is greater at the beginning of the input train than at the end. This reduction of inward current resulting from I_h deactivation is referred to as an “effective outward current.” This effective outward current increases during the course of the synaptic input train such that the excitatory drive on the neuron decreases. This reduction of excitatory drive also serves to decrease temporal summation. Interestingly, even though the deactivation of I_h increases R_{in} and thus increases τ_m, the net effect of I_h blockade is an increase in temporal summation due to the overwhelming effect of I_h blockade on τ_m at rest (see Magee 1999, 2000; Spruston et al., 1999).

For the experiments on temporal summation in SR/SLM neurons, extracellular stimulation was applied to the MF pathway and EPSP summation was measured for 50 Hz five pulse input trains. The extent of temporal summation was quantified by calculating a summation index: SI = ($EPSP_5$ – $EPSP_1$)/$EPSP_1$ where $EPSP_i$ is the amplitude of the i^{th} EPSP (Magee, 1999). For all cells (n = 4), the addition of 50 μM ZD7288 resulted in an increase in temporal summation. On average, the SI increased from 1.33 ± 1.12 under baseline conditions to 2.6 ± 0.56 when ZD7288 was present (Fig 8). However, the effect of ZD72880 was not significant as determined by a paired-samples t-test (p = 0.102), likely because of the high variability in the SI measures. It should be noted that because MF inputs terminate on the dendrites of CA3 interneurons (Acsády et al., 1998; Calixto et al., 2008), and immunolabeling HCN subunits appears solely in somata of SR/SLM interneurons (data not shown), the summation responses may be affected by voltage gated channels in the dendrites. For instance, the temporal summation increases following ZD7288 application might be partially accounted for by the activation of other channels that are activated due to the increase in response amplitude due to I_h blockade. For instance, Calixto and colleagues (2008) have found evidence for T-type calcium channels in the dendrites of SLM interneurons that increase temporal summation of sequentially evoked MF-PP responses.

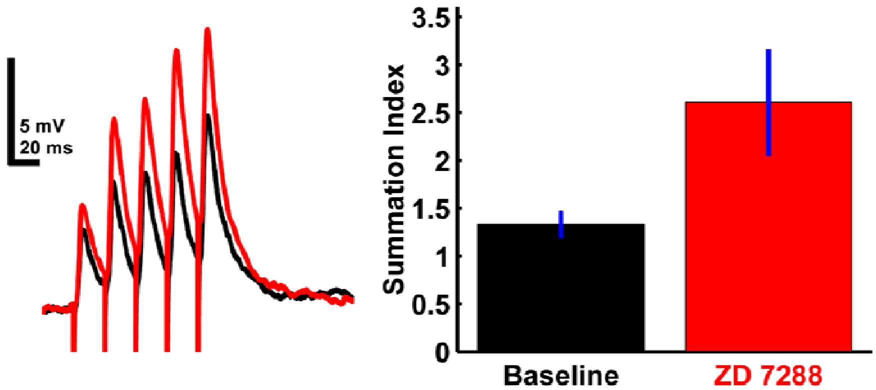

Figure 8. I_h *decreases temporal summation*. A single cell example of responses to 50 Hz MF stimulation is shown under baseline (black) and ZD7288 (red) conditions. Means are plotted on the right.

3.3.2. *Frequency Domain Experiments*

Rhythmic activity in populations of neurons reflected by extracellular recordings has been shown to be associated with cognitive functions of the hippocampus (e.g., Buzsáki, 2002, 2005). While the mechanisms whereby population rhythmic activity is generated are not completely characterized, it is generally believed that some combination of neural network characteristics (e.g., spike timing of distinct inhibitory cells, Klausberger & Somogyi, 2008) and intrinsic properties of individual neurons (e.g, the voltage dependent currents through ion channels) orchestrate the generation of these oscillations (e.g., Hutcheon & Yarom, 2000; Llinás, 1988). Subthreshold membrane resonance is an example of an intrinsic membrane property that is believed to be important for the transmission of rhythmic inputs in neural networks. For example, because some neurons have disparate resonant frequencies, the spiking of such neurons will correspond preferentially to inputs arriving at their respective resonance frequencies. The result of this is that different neurons can select for different input frequencies such that membrane resonance in part determines the rhythms a given neuron will likely contribute to.

As mentioned previously, I_h has been shown to confer subthreshold membrane resonance in neurons (e.g., Hutcheon et al., 1996). This is the result of the fact that I_h behaves as a "phenomenological inductance" in circuits with parallel resistance and capacitance, as in the neuronal membrane (see Erchova et al., 2004; Narayanan & Johnston, 2008). Thus I_h performs high-pass filtering of low frequency inputs due to the slow channel kinetics: low frequency inputs deactivate I_h during the depolarizing input phase and activate I_h during the hyperpolarizing input phase. The effective outward current resulting from I_h deactivation reduces the depolarizing voltage response to the depolarizing phase of inputs at low frequencies. Inward current resulting from I_h activation provides depolarizing drive that attenuates the hyperpolarizing effect of low frequency inputs. In general, for I_h with kinetics described by τ_h (V), the resonant frequency f_r will depend on the relation between τ_h and τ_m such that $(2\pi\tau_h)^{-1} < fr < (2\pi\tau_m)^{-1}$ (Hutcheon & Yarom, 2000). Therefore, the h-channel kinetics must be slower than the passive membrane time constant (i.e., $\tau_h > \tau_m$) for the generation of I_h mediated resonance.

To test the hypothesis that I_h imparts subthreshold membrane resonance to SR/SLM interneurons (Hutcheon & Yarom, 2000), ZAP stimuli (*Eq. 5*, Fig 9A) were applied at potentials where I_h is active. The voltage responses to these inputs (Fig 9B) were used to compute the frequency dependent impedance magnitude, |Z|(f) (Fig 9C, see Methods). Resonance is defined as a peak in the impedance magnitude-frequency (|Z|-f) function above the initial frequency (0.5 Hz). The extent of resonance is quantified by calculating the ratio of the impedance computed at the peak versus impedance at 0.5 Hz. The frequency where the impedance is at its peak value is referred to as the resonant frequency, f_r. The ratio $|Z|(f_r)/|Z|(0.5\ Hz)$ is referred to as the Q-factor (e.g., Hutcheon & Yarom, 2000). Therefore, when |Z|(f) decreases monotonically from |Z|(0.5 Hz), Q = 1 and there is no resonance, as is the case at -70 mV (Figs 9-11).

Impedance measurements were obtained at -70, -80, and -90 mV in the presence and absence of 50 μM ZD7288 (Fig 10). For all cells at -70, Q was equal to 1.0 in the absence (n = 6) and presence of ZD7288 (n = 3), indicating that I_h mediated resonance is not present at this potential. At -80 mV (n = 2) and -90 mV (n = 8), $f_r > 0.5$ Hz and Q > 1.0 for some cells (Figs 10,11) thus indicating resonance peaks at more hyperpolarized potentials. At -80 mV, f_r was 0.5 Hz for one cell and 1.26 Hz for the other. At -90 mV, $f_r = 0.5$ Hz was found for five neurons and f_r = 1.30, 1.49, and 3.05 Hz for the others (summary data presented in Fig 11). When ZD7288 was applied, the resonance is abolished at both -80 mV (n = 2) and -90 mV (n = 4) such that f_r = 0.5 Hz and Q = 1.0 for all cells.

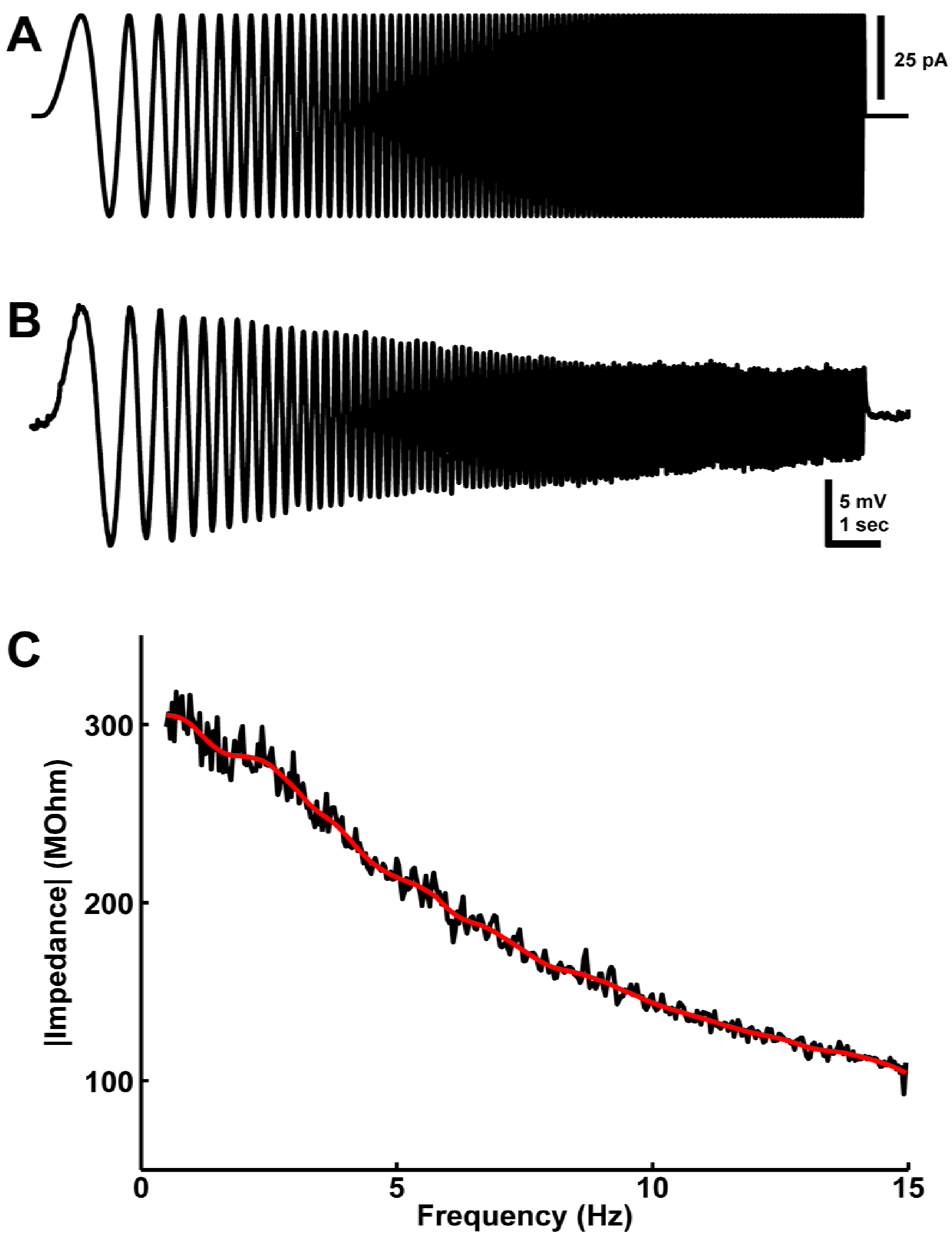

Figure 9. *Impedance measurements.* **A:** The waveform of the ZAP stimulus (*Eq. 5*). **B:** A typical response to I_{ZAP} at -70 mV. C: The impedance magnitude |Z| is plotted as a function of input frequency. The red trace shows the result of smoothing the noisy trace that was computed as $|Z| = |FFT(V)/FFT(I_{ZAP})|$.

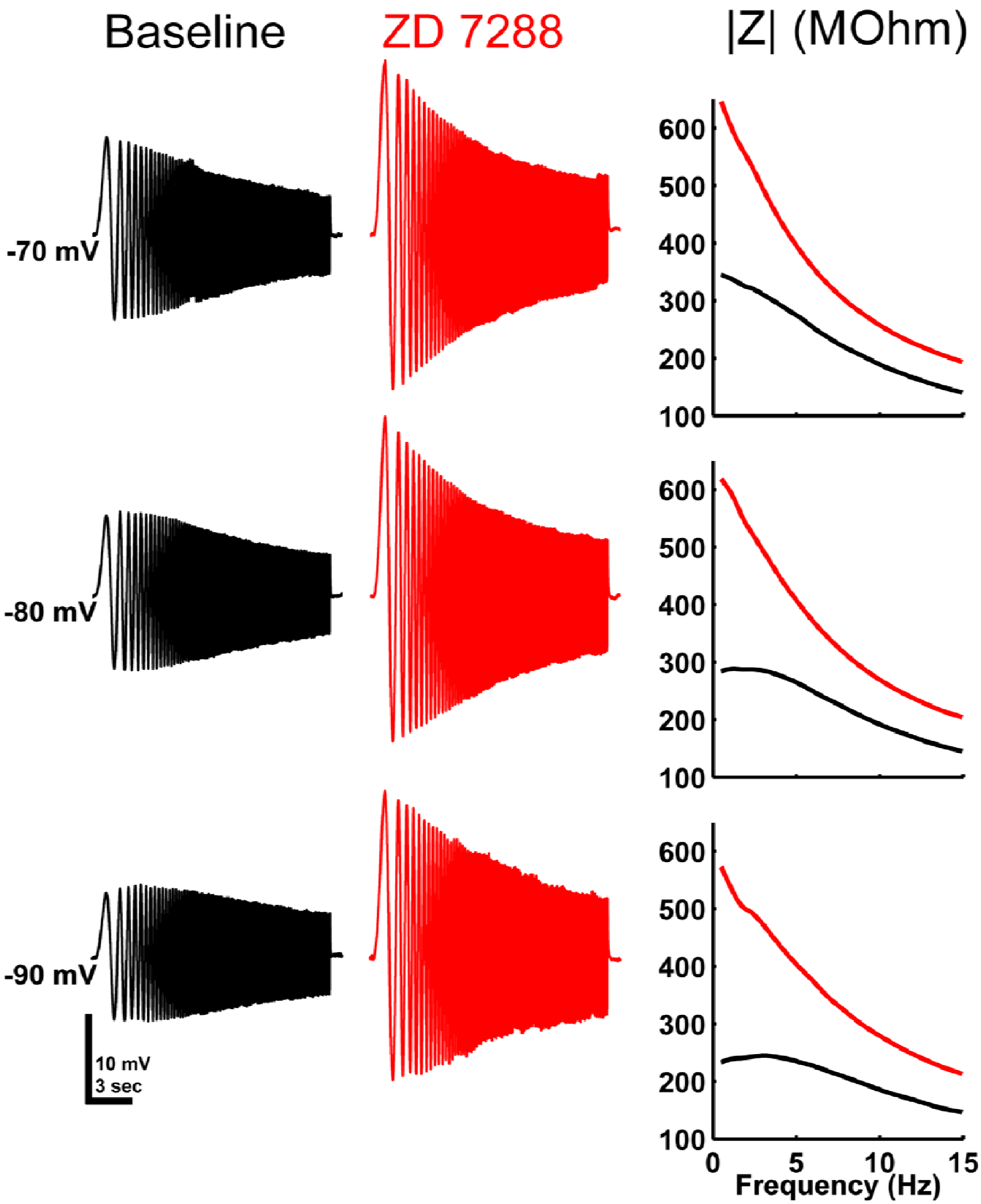

Figure 10. *Impedance measurements before and after I_h blockade.* Impedance measurements were obtained at -70, -80 and -90 mV and smoothed impedance magnitude traces were plotted. This representative example shows that ZD7288 application (red traces) increases |Z| at all potentials examined.

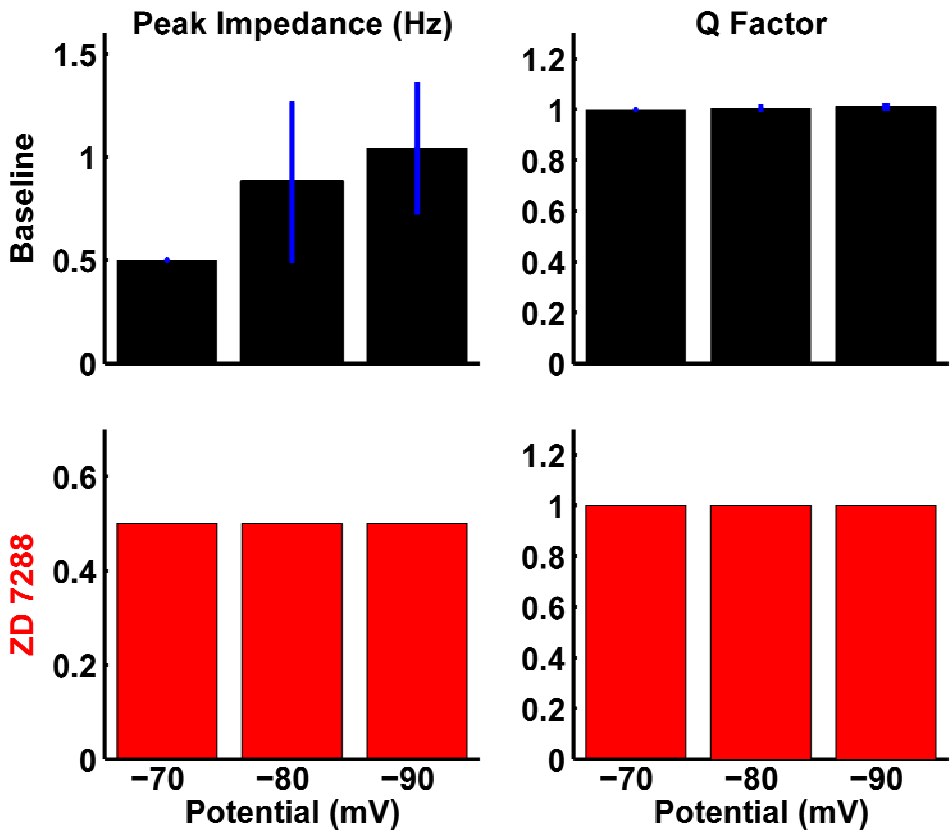

Figure 11. *Summary data for impedance measurements.* Mean f_r values (± SEM) are plotted on the left for baseline (top) and ZD7288 (bottom) conditions. Corresponding mean Q values are plotted on the right.

4.0 DISCUSSION

4.1 BIOPHYSICAL PROPERTIES OF IH IN SR/SLM INTERNEURONS

The reversal potential estimated for I_h in SR/SLM interneurons, E_h = -33.7 mV, was well within the range of E_h values previously reported, -20 to -40 mV, which corresponds to a pK:pNa permeability ratio between 3:1 and 5:1 (Robinson & Seigelbaum, 2003). For example, Maccaferri and McBain (1996) found E_h = -32.9 mV in CA1 interneurons from stratum oriens. Characteristics of the voltage dependence of I_h vary substantially among neurons from different preparations. The voltage at half-maximal activation ($V_{1/2}$) is -88.8 mV in SR/SLM interneurons and this value falls within the reported range for sigmoidal fits describing I_h activation. This $V_{1/2}$ estimate is relatively hyperpolarized compared to results some other reports. For instance, $V_{1/2}$ was estimated to be -84.1 mV in CA1 interneurons (Maccaferri & McBain, 1996), -83.9 mV in DG interneurons (Aponte et al., 2006), -76 to -73 mV in subicular pyramidal neurons (van Welie et al., 2006), -77 mV in EC stellate cells (Dickson et al., 2000), -81 mV in visual cortex pyramidal neurons (Solomon & Nerbonne, 1993a), -74.6 mV for thalamic neurons (McCormick & Pape, 1990), and -75.7 in neurons from the medial nucleus of the trapezoid body (MNTB, Banks et al., 1993). In contrast, $V_{1/2}$ estimates are more hyperpolarized in other cells: $V_{1/2}$ = -86.0 mV in prefrontal cortex interneurons (Wu & Hablitz, 2005) and -89.5 mV in dendritic sites of CA1 pyramidal neurons (Magee, 1998).

It is possible that the relatively hyperpolarized activation function results from intracellular washout of cyclic nucleotides. The voltage dependent activation functions for h-currents mediated by HCN2 and/or HCN4 subunits are shifted towards more hyperpolarized potentials when cyclic nucleotides are not present in the bathing solutions of inside-out patch recordings (Chen et al., 2001). For example, when HCN1 and HCN2 were co-expressed in oocytes, $V_{1/2}$ values measured from inside-out patches were shifted 13 mV in the hyperpolarized direction in the absence of cAMP (Chen et al., 2001). For reduction of cyclic nucleotide modulation to explain the relatively hyperpolarized $V_{1/2}$ value observed in my study, HCN2 and/or HCN4 would need to partially compose I_h in SR/SLM interneurons. Preliminary immunohistochemical data indicate that all four HCN subunits are expressed in somata of SLM interneurons (data not shown). Thus, $V_{1/2}$ = -88.8 mV could be due to reduction of cyclic nucleotide binding to HCN2/4 subunits following whole-cell break in. It could also be the case that the hyperpolarized $V_{1/2}$ is due to current rundown (Pape, 1996; Robinson & Seigelbaum, 2003). DiFrancesco and colleagues (1986) observed substantial leftward shifts in the voltage dependence of I_h activation (40 to 50 mV) during prolonged whole-cell recordings; however, these shifts were not apparent until at least 20 minutes after break-in. This rundown is not likely to account for our activation function because initial I_h measurements were obtained 10-15 minutes after break-in, after which I_h was antagonized by ZD 7288 perfusion. It has been determined that I_h rundown occurs in the preparation used for my experiments between 10 and 25 minutes after break-in (Anderson et al., 2008), but it has not been determined whether rundown occurs between 10 and 15 minutes. So I cannot completely rule out the possibility that I_h rundown partially affected my measurements.

The slope factor used in the sigmoidal fit to the normalized steady state conductance values obtained from my measurements was k = 10 mV. This falls within the range of typical k values, although it indicates a somewhat shallow slope relative to some activation functions (lower k values correspond to steeper activation functions). Fitted k values from previous analyses were 8 to 9 mV in CA1 pyramidal neurons (Magee, 1998), 8.7 to 8.8 mV in subicular neurons (van Welie et al., 2006), 7.2 mV in visual cortex pyramidal neurons (Solomon & Nerbonne, 1993a), 5.5 mV for thalamic neurons (McCormick & Pape, 1990), and 5.7 in neurons from the MNTB (Banks et al., 1993). However, other fits for this parameter gave values around 10 mV or larger: k = 10.2 in CA1 interneurons (Maccaferri & McBain, 1996), 13.1 mV in DG interneurons (Aponte et al., 2006), and 11.2 mV in EC stellate cells (Dickson et al., 2000). Hence, the parameters of our activation function ($V_{1/2}$ and k) are highly consistent with the available literature. Even though $V_{1/2}$ = -88.8 mV is relatively negative, this value falls within the range of reported values for intact cells (~ -60 to -90 mV, Robinson & Seigelbaum, 2003; Pape, 1996).

Another interesting result regarding my biophysical analysis of I_h in SR/SLM interneurons was that the sigmoidal fit to the normalized conductance values was statistically superior (i.e., the R^2 for the model fit to the data was larger) if a voltage-independent component was added (*Eq. 1*). I found that the voltage-independent component comprised 8% of the activation function. Most analyses of I_h use sigmoidal curves without voltage-independent components, though statistical comparisons were not made in these studies between these fits and fits with equations containing a voltage-independent term (e.g., Banks et al., 1993; Chen et al., 2001; Maccaferri & McBain, 1996; Solomon & Nerbonne, 1993b). In a recent report describing the properties of I_h in DG interneurons, Aponte and colleagues (2006) also used *Eq. 1* for their activation function and found that the voltage-independent component comprised 8% of the function, identical to my finding. Other investigators also found evidence for a voltage-independent component of I_h based on instantaneous currents following hyperpolarizing voltage steps from depolarized potentials where I_h generally is not thought to be active (Day et al., 2005; Rodrigues & Oertel, 2006). Instantaneous components of I_h were originally described when HCN2 subunits were expressed in heterologous system (Proenza et al., 2002). It was later found that the instantaneous component of I_h could be blocked independent of the time dependent component by rapidly applying Cd^{2+} (Proenza & Yellen, 2006). This finding was interpreted as evidence that there are two distinct populations of h-channels: a voltage-dependent and a voltage-independent channel population.

Consistent with several previous reports from intact neurons and heterologous expression systems, the kinetics of I_h activation and deactivation in SR/SLM interneurons were characterized by double-exponential time courses (e.g., Banks et al., 1993; Chen et al., 2001; Maccaferri & McBain, 1996; Solomon & Nerbonne, 1993b). The kinetic functions were voltage dependent such that activation rates increased with hyperpolarization (Pape, 1996; Robinson & Seigelbaum, 2003) while deactivation kinetics were relatively less voltage sensitive. It was also found that the activation and deactivation exponential time constants could be described by distinct functions of voltage and this was the case for both fast and slow time constants (Fig 3A,B). Interestingly, I_h deactivation was faster than activation of the current, as is apparent from some plots of activation and deactivation currents in previous reports (Angelo et al., 2007; Aponte et al., 2006; Magee, 1998; McCormick & Pape, 1990; Williams & Stuart, 2000). It was also found that the contribution of the fast component of I_h increased with hyperpolarization and fast components were generally >50% of the total activated or deactivated current, similar to findings for HCN1 and HCN2 (Chen et al., 2001). It is worth noting that deactivation kinetics were not assessed via curve fitting in many reports (e.g., Banks et al., 1993; Chen et al., 2001; Maccaferri & McBain, 1996; van Welie et al., 2006). When reported, deactivation kinetics were generally characterized by a single exponential time course (Aponte et al., 2006; Magee, 1998; McCormick & Pape, 1990; Solomon & Nerbonne, 1993b; Williams & Stuart, 2000). Our finding that the fractional contribution of fast deactivation comprises ~60% of I_h deactivation at -60 mV is a novel finding suggesting that the rapid time course component of deactivation at potentials positive to V_{rest} is important for the effects of I_h on synaptic integration.

4.2 MODELING AND DYNAMIC CLAMP OF IH

I_h is typically modeled by ether a standard HH model or a variation of the HH formalism. For instance, Dickson and colleagues (2000) modeled I_h using the HH conventions by fitting the activation and deactivation traces to obtain state transition variables. As in the original specification of the model (Hodgkin & Huxley, 1952), h-current traces were fitted with kinetic and fractional activation parameters to obtain the gate transition rate values $\alpha(V)$ and $\beta(V)$: $\alpha(V) = X_\infty(V) / \tau_h(V)$ and $\beta(V) = (1 - X_\infty(V)) / \tau_h(V)$. These values were fitted and the resulting functions were then used to obtain the time constant and normalized steady state conductance functions: $\tau_h(V) = (\alpha(V) + \beta(V))^{-1}$ and $X_\infty(V) = \alpha(V)\,(\alpha(V) + \beta(V))^{-1}$ (Hodgkin & Huxley, 1952). Using these functions, the gating variable for I_h is computed as in this report, $\tau_h(V)\, dX/dt = X_\infty(V) - X$. Alternatively, as in the present study, I_h is often modeled using a variant of the HH model where $\tau_h(V)$ and $X_\infty(V)$ are independent (e.g., Angelo et al., 2007). In these models,

$X_\infty(V)$ is obtained by fitting sigmoidal curves to either the normalized steady state conductance values (e.g., Aponte et al., 2006) or the normalized tail currents obtained following the termination of hyperpolarizing pulses (e.g., Williams & Stuart, 2000). The kinetics are determined by fitting the activation and deactivation time constant values with a function of voltage to obtain $\tau_h(V)$. The main difference between these models and the original HH model is that $\tau_h(V)$ and $X_\infty(V)$ are not jointly determined by a set of rate functions, $\alpha(V)$ and $\beta(V)$ (Angelo et al., 2007; Hodgkin & Huxley, 1952).

HH models of I_h have been adapted to accommodate I_h with activation and deactivation exponential time courses characterized by two time constants, as in the present study (Dickson et al., 2000; Hutcheon et al., 1996). In these models, two time constant functions were fitted to the relations between the time constants and voltage: $\tau_{h,f}(V)$ and $\tau_{h,s}(V)$ describe the fast and slow time courses of I_h activation/deactivation. Correspondingly, two gating variables were used, the kinetics of which were described by these time constant functions: X_f and X_s. The normalized conductance was computed by multiplying the fast and slow gating variables, respectively, by the fractional contributions of the fast and slow components of I_h and taking the sum of these values: $X = X_f F + X_s(1 - F)$. Thus, in these models, two gating variables are updated according to their respective time constants and the normalized conductance is computed by weighting each gating variable by the fractional contribution of its kinetic component.

The model of I_h presented in this paper departs from the aforementioned model with two kinetic components (Dickson et al., 2000; Hutcheon et al., 1996) because the activation and deactivation kinetics were characterized by distinct functions of voltage for both exponential components (Fig 3), as is apparent in other reports (Angelo et al., 2007; Aponte et al., 2006; Magee, 1998; McCormick & Pape, 1990; Williams & Stuart, 2000). Hence, this model is a novel extension of the HH formalism that can be used to describe a voltage-dependent conductance that activates and deactivates with distinct time courses. In order to model I_h with these characteristics, two gating variables were used, X_f and X_s, as in previous reports. However, a logical statement was evaluated at each simulation time step in order to determine whether the gating variables X_f and X_s should be updated based on the activation or deactivation kinetics. The fractional conductance variable X was compared with the normalized steady state conductance X_∞ at each time step and if X was less than or equal to X_∞, then the gating variables were updated using the activation kinetics and X was computed based on the updated gating variables and the corresponding fractional contributions of each component (see Appendix A). For $X > X_\infty$, the channel population was considered to be undergoing deactivation and the gating variables (X_f and X_s) and X values were computed accordingly.

The implementation of this model in simulations and dynamic clamp experiments indicates that it provides a qualitatively accurate portrayal of I_h in real time at a sampling frequency of 10 kHz (dt = 100 μs in simulations). Hence, our model can be readily applied in simulations of I_h where voltage clamp measurements from a given preparation suggest that I_h kinetics have double exponential time courses that are distinct for activation and deactivation.

4.3 FUNCTIONAL IMPLICATIONS

Experiments were conducted to evaluate the biological significance of I_h at subthreshold membrane potentials near V_{rest} in SR/SLM interneurons. In particular, I focused on the role of I_h in modulating the temporal summation of MF input and neuronal responses to oscillatory inputs with frequency variation. The temporal summation data replicated previous findings indicating that I_h reduces the temporal summation of 50 Hz input (Magee, 1998, 1999). In general, a reduction of temporal summation is associated with an increased sensitivity of input timing such that action potential output occurs preferentially for synchronized synaptic inputs. Increases in temporal summation associated with I_h blockade results in less temporally selective firing to coincident or synchronized inputs (Magee, 1999; Yamada et al., 2005). For example, because I_h decreases the EPSP decay time constant via its reduction of input resistance and effective outward current resulting from channel deactivation (Magee, 1998, 1999), a given train of inputs would need to be activated a higher rate (i.e., input would need to be more synchronized) to bring the membrane to action potential in the presence of I_h compared to conditions under I_h blockade. Alternatively, because a 5-pulse 50 Hz train results in less summation in the presence of I_h, larger input amplitudes would need to be evoked to reach threshold for this input train relative to the condition in which I_h is blocked. The proposed functional implication of this I_h mediated reduction of temporal summation is that I_h promotes "coincidence detection" (Magee, 1999).

The term coincidence detection refers a mode of synaptic integration in which spikes are generated preferentially following coincident or highly synchronized input. Coincidence detection is generally contrasted with the "temporal integration" mode of synaptic integration in which spiking can occur following the summation of many sequentially activated asynchronous inputs (Konig et al., 1996; Shadlen & Newsome, 1994; Softky, 1995). Several factors have been shown to foster coincidence detection including feedforward inhibition (Pouille & Scanziani, 2001), the kinetic properties of postsynaptic ionotropic receptors, and the passive and active properties of the neuronal membrane (e.g., Spruston et al., 1999; Spruston, 2008). Evidence for coincidence detection of excitatory input has been found in the auditory brain stem (Yamada et al., 2005), visual cortex (Azouz & Gray, 2000, 2003), somatosensory cortex (e.g, Wilent & Contreras, 2004), and hippocampus (e.g., Pouille & Scanziani, 2001). The proposed functions of coincidence detection vary depending on the brain region and cell type under consideration.

The I_h mediated coincidence detection in SR/SLM interneurons might be important for propagating precisely timed inhibition to CA3 in order to support temporally coordinated firing in CA3 pyramidal cells. However, because these interneurons have axons that mainly project towards the hippocampal fissure (Ascoli et al., 2009), their firing might primarily serve to shunt inputs from the entorhinal cortex and/or prevent the induction of LTP at RC synapses. The precisely timed inhibition of dendritic segment where RC synapses are located could provide sparcification of the incoming cortical representation by reducing the activity level in CA3 in addition to the pattern separating operations of the DG (Acsády & Káli, 2007). The selective inhibition preventing LTP of RC synapses would reduce the number of synapses encoding a given event, thus enhancing pattern separation. Further, precisely timed inhibition of CA3 during the presentation of a partial cue for a previously stored memory could reduce the "noise" in the activated ensemble by reducing the efficacy of RC synapses that were not potentiated for the original input pattern associated with the partial cue, therefore reducing activity of cells that were not part of the original representation.

In addition to evaluating the influences of I_h on the characteristics of subthreshold synaptic integration, I examined the possibility that I_h confers membrane resonance to SR/SLM interneurons at V_{rest} and more hyperpolarized potentials. Sinusoidal current injections were applied from the patch pipette and impedance measurements were obtained by applying Fourier analyses to the current input and voltage response waveforms. At approximately V_{rest} (-70 mV), there was no peak in the impedance magnitude-frequency (|Z|-f) function beyond the initial frequency for which |Z| was computed (0.5 Hz), and hence the Q values were 1.0 for all cells (Figs 9-11). When |Z| measures are obtained from neurons held at -80 or -90 mV, peaks became apparent in the |Z|-f functions at frequencies greater than 0.5 Hz for some neurons. In all such cases, however, the associated Q values were <1.1. While there is not a generally accepted criterion for defining the presence of resonance from a |Z|-f function, very low Q values suggest that $|Z|(f_r)$ is very close to |Z|(0.5 Hz) and the voltage response is not substantially greater for oscillatory inputs at f_r than at lower frequencies. Erchova and colleagues (2004) used the criterion of Q > 1.2 to designate the presence of resonance, for example. Thus, because the Q values were very low for SR/SLM interneurons (~1.0), I do not consider these neurons to possess subthreshold resonance at potentials where I_h is active. For comparison, impedance measurements from other neurons based on the ZAP current inputs at potentials between -60 and -80 mV indicated the following average estimates of f_r and Q: f_r = 3.0 and Q = 1.32 for hippocampal CA1 pyramidal neurons (at -80 mV, Hu et al., 2006), f_r = 10.6 Hz and 1.2 < Q < 2.1 for entorhinal cortex stellate cells (at ~ -60 mV, Erchova et al., 2004; see also Hass et al., 2007), and f_r = 1.3 Hz and Q = 1.3-1.4 for neocortical sensorimotor pyramidal neurons (at -70 mV, Hutcheon et al., 1996). For all cell types, the expression of resonance at these potentials was abolished by I_h blockade with either Cs^+ or ZD7288. Only two reports have described |Z| measurements from recordings of putative interneurons (Hutcheon et al., 1996; Pike et al., 2000). In the neocortex, fast spiking neurons did not show resonance in the theta band. When hippocampal area CA1 was examined, it was found that fast-spiking cells showed resonance near or within the gamma band (f_r = 30-50 Hz) while regular spiking putative interneurons showed theta band resonance (f_r = 2-7 Hz, Pike et al., 2000). However, the recordings from CA1 were obtained at potentials near the action potential threshold where I_h was probably not activated/deactivated by the ZAP input. Hence this document describes the first analysis of frequency domain properties of hippocampal interneurons at subthreshold potentials where I_h is expected to have an influence.

Pharmacological blockade of I_h resulted in an alteration of the impedance function at all potentials at which ZAP stimuli were applied (Fig 10). First, the maximal impedance was increased substantially, which is likely to be the result of decreasing the input conductance. Further, the steepness of the $|Z|$ function at low frequencies between $f = 0.5$ and $f \sim 7$ Hz was increased when I_h was blocked. This “flattening” effect of I_h on the $|Z|$ functions was more pronounced as hyperpolarization was increased. These results suggest that even though I_h does not confer veritable resonance to SR/SLM interneurons, I_h affects the frequency domain properties of the interneurons such that the frequency dependence of response amplitude is attenuated (compare the slopes of impedance functions in Fig 10 with and without ZD7288). This reduction of low-pass filtering at frequencies within the theta band (~4 – 10 Hz) may be important because bursts of excitatory input from PP and MF inputs arrive at theta frequencies during the encoding and retrieval of spatial information. However, because the theta band firing rates of hippocampal neurons vary depending on contextual factors such as movement speed (e.g., see McNaughton et al., 1983; Slawínska & Kasicki, 1998) there is likely jitter in the frequency at which input barrages arrive in CA3. The reduced sensitivity to input frequency when I_h is present might help to normalize the integrative properties of the interneurons with respect to input frequency. This indicates that, in general, there is little variation in the inhibitory tone in CA3 pyramidal cell dendrites with respect to input frequency. The importance of these results appears to be that these SR/SLM neurons apply consistent inhibition without regard to behavior state dependent rhythmic activity frequency variations.

4.4 SUMMARY

This thesis described the results of experiments that were designed to determine the properties and functions of I_h in SR/SLM interneurons. The biophysical characterization of I_h indicates that channel deactivation occurs more rapidly than activation while both are characterized by double exponential functions. A novel finding was that the fast component of deactivation is ~60% of the deactivated current at -60 mV. This rapid deactivation is likely to be an important contributing factor to the I_h mediated reduction of temporal summation described here. The biophysical properties determined by fitting curves to voltage clamp traces were incorporated into a novel extension of the Hodgkin-Huxley scheme for modeling voltage gated channel population activity. The functionality of this model was supported by current and voltage clamp simulations, as well as dynamic clamp experiments. This model could be very useful for investigating the influences of I_h properties on neuronal function in simulations. The temporal summation experiments and model simulations suggest that I_h supports sensitivity to input timing favoring synchronous input. Finally, the impedance measurements suggest that SR/SLM interneurons do not exhibit subthreshold resonance near rest, indicating that these cells do not selectively amplify input within a certain bandwidth. In contrast, I_h appears to reduces the low-pass filtering of the neuronal membrane and effectively support the normalization of response amplitude to oscillating input with respect to frequency.

APPENDIX A

PSEUDO-CODE FOR THE ALGORITHM USED TO COMPUTE IH

The following pseudo-code illustrates how the I_h computations were made in current clamp simulations within a for-loop at time t:

$X(t - dt) = (X_f(t - dt)\ F(t - dt) + X_s(t - dt)\ (1 - F(t - dt)))$

IF $\quad X(t - dt) \leq X_\infty(t)$

THEN

$F(t) = F_{A,f}(t)$
$X_f(t) = X_f(t - dt) + (dt / \tau_{A,f}(t))\ (X_\infty(t) - X_f\ (t - dt))$
$X_s(t) = X_s(t - dt) + (dt / \tau_{A,s}(t))\ (X_\infty(t) - X_s\ (t - dt))$
$X(t) = (X_f(t)\ F_{A,f}(t) + X_s(t)\ (1 - F_{A,f}(t)))$
$I_h(t) = g_{h,max}\ X(t)\ (V(t - dt) - E_h)$

ELSE

$F(t) = F_{D,f}(t)$
$X_f(t) = X_f(t - dt) + (dt / \tau_{D,f}(t))\ (X_\infty(t) - X_f\ (t - dt))$
$X_s(t) = X_s(t - dt) + (dt / \tau_{D,s}(t))\ (X_\infty(t) - X_s\ (t - dt))$
$X(t) = (X_f(t)\ F_{D,f}(t) + X_s(t)\ (1 - F_{D,f}(t)))$
$I_h(t) = g_{h,max}\ X(t)\ (V(t - dt) - E_h)$

$V(t) = V(t - dt)\ - (dt/C_m)(I_h(t) + g_L(V(t - dt) - E_L)) + (dt/C_m)I_{ext}$

BIBLIOGRAPHY

Acsády, L., Kamondi, A., Sik, A., Freund, T.F., & Buzsaki, G. (1998). GABAergic cells are the major postsynaptic targets of mossy fibers in the rat hippocampus. *The Journal of Neuroscience, 18*, 3386-3404.

Amaral., D.G., Ishizuka, N., & Claiborne, B. (1990). Neurons, numbers and the hippocampal network. *Progress in Brain Research, 83*, 1-11.

Amaral, D.G., & Witter, M.P. (1995). Hippocampal formation. In: *The Rat Nervous System* (G. Paxinos, Ed.). San Diego: Academic Press, pp 443-493.

Anderson, W.D., Galván, E.J., & Barrionuevo, G. (2008). Modification of I_h following mossy fiber LTP induction. *Society for Neuroscience Meeting*, Washington, DC, 240.13/E35.

Angelo, K., London, M., Christensen, S.R., & Häusser, M. (2007). Local and global effects of I_h distribution in dendrites of mammalian neurons. *The Journal of Neuroscience, 27*, 8643-8653.

Aponte, Y., Lien C-C., Reisinger, E., & Jonas, P. (2006). Hyperpolarization-activated cation channels in fast-spiking interneurons of rat hippocampus. *Journal of Physiology, 574*, 229-243.

Ascoli, G.A., Brown, K.M., Calixto, E., Card, J.P., Galván, E.J., Perez-Rosello, T., & Barrionuevo, G. (2009). Quantitative morphometry of electrophysiologically identified CA3b interneurons reveals robust local geometry and distinct cell classes. *Journal of Comparative Neurology, 515*, 677-695.

Azouz, R., & Gray, C.M. (2000). Dynamic spike threshold reveals a mechanism for synaptic coincidence detection in cortical neurons in vivo. *Proceedings of the National Academy of Sciences, 97*, 8110-8115.

Bader, C.R., Bertrand, D., & Schwartz, E.A. (1982). Voltage-activated and calcium-activated currents studied in solitary rod inner segments from the salamander retina. *Journal of Physiology, 331*, 253-284.

Banks, M.I., Pearce, R.A., & Smith, P.H. (1993). Hyperpolarization-activated cation current (I_h) in neurons of the medial nucleus of the trapezoid body: Voltage-clamp analysis and enhancement by norepinephrine and cAMP suggest a modulatory mechanism in the auditory brain stem. *Journal of Neurophysiology, 70*, 1420-1432.

Berger, T., Larkum, M.E., & Lüscher, H-R. (2001). High I_h channel density in distal apical dendrite of layer V pyramidal cells increases bidirectional attenuation of EPSPs. *Journal of Neurophysiology, 85*, 855-868.

Bobker, D.H., & Williams, J.T. (1989). Serotonin augments the cationic current I_h in central neurons. *Neuron, 2*, 1535-1540.

Boss, B., Peterson, G., Cowan, W. (1985). On the numbers of neurons in the dentate gyrus of the rat. *Brain Research, 338*, 144-150.

Boss, B., Turlejski, K., Stanfield, B., & Cowan, W. (1987). On the numbers of neurons in fields CA1 and CA3 of the hippocampus of Sprague-Dawley and Wistar rats. *Brain Research, 406*, 280-287.

Brown, H.F., Difrancesco, D., & Nobel, S.J. (1979). How does adrenaline accelerate the heart? *Nature, 280*, 235-236.

Buzsáki, G. (2002). Theta oscillations in the hippocampus. *Neuron, 33*, 325-340.

Buzsáki, G. (2005). Theta rhythm of navigation: Link between path integration and landmark navigation, episodic and semantic memory. *Hippocampus, 15*, 827-840.

Calixto, E., Galván, E.J., Card, J.P., & Barrionuevo, G. (2008). Coincidence detection of convergent perforant path and mossy fibre inputs by CA3 interneurons. *Journal of Physiology, 586*, 2695-2712.

Carnevale, N.T., Tsai, K.Y., Claiborne, B.J., & Brown, T.H. (1997). Comparative electrotonic analysis of three classes of rat hippocampal neurons. *Journal of Neurophysiology, 78*, 703-720.

Chen, S., Wang, J., & Seigelbaum, S.A. (2001). Properties of hyperpolarization-activated pacemaker current defined by coassembly of HCN1 and HCN2 subunits and basal modulation by cyclic nucleotide. *Journal of General Physiology, 117*, 491-503.

Clapham, D.E. (1998). Not so funny anymore: Pacing channels are cloned. *Neuron, 21*, 5-7.

Day, M., Carr, D.B., Ulrich, S., Ilijic, E., Tkatch, T., & Surmeier, D.J. (2005). Dendritic excitability of mouse frontal cortex pyramidal neurons is shaped by the interaction among HCN, Kir2, and K_{leak} channels. *The Journal of Neuroscience, 25*, 8776-8787.

Dickson, C.T., Magistretti, J., Shalinsky, M.H., Fransén, E., Hasselmo, M.E., & Alonso, A. (2000). Properties and role of I_h in the pacing of subthreshold oscillations in entorhinal cortex layer II neurons. *Journal of Neurophysiology, 83*, 2562, 2579.

DiFrancesco, D. (1981). A study of the ionic nature of the pace-maker current in calf purkinje fibers. *Journal of Physiology, 314*, 377-393.

DiFrancesco, D., Ferroni, A., Mazzanti, M., & Tromba, C. (1986). Properties of the hyperpolarization-activated current (i_f) in cells isolated from the rabbit sino-atrial node. *Journal of Physiology, 377*, 61-88.

DiFrancesco, D., & Tortora, P. (1991). Direct activation of cardiac pacemaker channels by intracellular cyclic AMP. *Nature, 351*, 145-147.

DiFrancesco, D & Tromba, C. (1988a). Inhibition of the hypolarization-activated current (i_f) induced by acetylcholine in rabbit sino-atrial node myocytes. *Journal of Physiology, 405*, 477-491.

DiFrancesco, D & Tromba, C. (1988b). Muscarinic control of the hypolarization-activated current (i_f) in rabbit sino-atrial node myocytes. *Journal of Physiology, 405*, 493-510.

Eichenbaum, H., & Otto, T. (1992). The hippocampus – What does it do? *Behavioral and Neural Biology, 57*, 2-36.

Erchova, I., Kreck, G., Heinemann, U., & Hers, A.V.M. (2004). Dynamics of rat entorhinal cortex layer II and III cells: Characteristics of membrane potential resonance at rest predict oscillation properties near threshold. *Journal of Physiology, 560*, 89-110.

Freund, T.F., & Buzsaki, G. (1996). Interneurons of the hippocampus. *Hippocampus, 6*, 347-470.

Gauss, R., Seifert, R., & Kaupp, U.B. (1998). Molecular identification of a hyperpolarization-activated channel in sea urchin sperm. *Nature, 393*, 583-587.

Hájos, N., Pálhalmi, J., Mann, E.O., Németh, B., Paulsen, O., & Freund, T.F. (2004). Spike timing of distinct types of GABAergic interneuron during hippocampal gamma oscillations *in vitro*. *The Journal of Neuroscience, 24*, 9127-9137.

Halliwell, J.V., & Adams, P.R. (1982). Voltage-clamp analysis of muscarinic excitation in hippocampal neurons. *Brain Research, 250*, 71-92.

Hass, J.S., Dorval II, A.D., & White, J.A. (2007). Contributions of I_h to feature selectivity in layer II stellate cells of the entorhinal cortex. *Journal of Computational Neuroscience, 22*, 161-171.

Hebb, D.O. (1949). *The Organization of Behavior: A Neuropsychological Theory*. New York: Wiley.

Henze, D.A., Wittner, L., & Buzsáki, G. (2002). Single granule cells reliably discharge targets in the hippocampal CA3 network *in vivo*. *Nature Neuroscience, 5*, 790-795.

Henze, D.A., Urban, N.N., & Barrionuevo, G. (2000). The multifarious hippocampal mossy fiber pathway: A review. *Neuroscience, 98*, 407-427.

Hodgkin, A.L., & Huxlex, A.F. (1952). A quantitative description of membrane current and its application to conduction and excitation in nerve. *Journal of Physiology, 117*, 500-544.

Hopfield, J.J. (1982). Neural networks and physical systems with emergent collective computational abilities. *Proceedings of the National Academy of Sciences, 79*, 2554-2558.

Hu, H., Vervaeke, K., & Storm, J.F. (2006). Two forms of electrical resonance at theta frequencies, generated by M-current, h-current and persistent Na^+ current in rat hippocampal pyramidal cells. *Journal of Physiology, 545*, 783-805.

Hutcheon, B., Miura, R.M., & Puil, E. (1996). Models of subthreshold membrane resonance in neocortical neurons. *Journal of Neurophysiology, 76*, 698-714.

Hutcheon, B., & Yarom, J. (2000). Resonance, oscillation and the intrinsic frequency preferences of neurons. *Trends in Neurosciences, 23*, 216-222.

Ishii, T.M., Takano, M., & Ohmori, H. (2001). Determinants of activation kinetics in mammalian hyperpolarization-activated cation channels. *Journal of Physiology, 537*, 93-100.

Ishii, T.M., Takano, M., Xie, L-H., Noma, A., & Ohmori, H. (1999). Molecular characterization of the hyperpolarization-activated cation channel in rabbit heart sinoatrial node. *The Journal of Biological Chemistry, 274*, 12835-12839.

Jung, M.W., & McNaughton, B.L. (1993). Spatial selectivity of unit activity in the hippocampal granule layer. *Hippocampus, 3*, 165-182.

Klausberger, T., & Somogyi, P. (2008). Neuronal diversity and temporal dynamics: The unity of hippocampal circuit operations. *Science, 321*, 53-57.

König, P., Engel, A.K., & Singer, W. (1996). Integrator or coincidence detector? The role of the cortical neuron revisited. *Trends in Neurosciences, 19*, 130-137.

Kullmann, P.H.M. Wheeler, D.W., Beacom, J., & Horn, J.P. (2004). Implementation of a fast 16-bit dynamic clamp using LabVIEW-RT. *Journal of Neurophysiology, 91*, 542-554.

Llinás, R.R. (1988). The intrinsic electrophysiological properties of mammalian neurons: Insights into central nervous system function. *Science, 242*, 1654-1664.

Ludwig, A., Zong, X., Jeglitsch, M., Hofmann, F., & Biel, M. (1998). A family of hyperpolarization-activated mammalian cation channels. *Nature, 393*, 587-591.

Maccaferri, G., & McBain, C.J. (1996). The hyperpolarization-activated current (I_h) and its contribution to pacemaker activity in rat CA1 hippocampal stratum oriens-alveus interneurons. *Journal of Physiology, 497*, 119-130.

Maccaferri, G., Mangoni, M., Lazzari, A, & DiFrancesco, D. (1993). Properties of hyperpolarization-activated current in rat hippocampal CA1 pyramidal cells. *Journal of Neurophysiology, 69*, 2129-2136.

Magee, J.C. (1998). Dendritic hyperpolarization-activated currents modify the integrative properties of hippocampal CA1 pyramidal neurons. *The Journal of Neuroscience, 18*, 7613-7624.

Magee, J.C. (1999). Dendritic I_h normalized temporal summation in hippocampal CA1 neurons. *Nature Neuroscience, 2*, 508-514.

Magee, J.C. (2000). Dendritic integration of excitatory synaptic input. *Nature Reviews Neuroscience, 1*, 181-190.

Mainen, Z.F., & Sejnowski, T.J. (1996). Influence of dendritic structure on firing patterns in model neocortical neurons. *Nature, 382*, 363-366.

Marr, D. (1969). A theory of cerebellar cortex. *Journal of Physiology London, 202*, 437-470.

Marr, D. (1971). Simple memory: A theory of archicortex. *Philosophical Transactions of the Royal Society of London B, 262*, 23-81.

McCormick, D.A., & Pape, H-C. (1990). Noradreneric and serotonergic modulation of a hyperpolarization-activated cation current in thalamic relay neurons. *Journal of Physiology, 431*, 319-342.

McNaughton, B.L., Barnes, C.A., & O'Keefe, J. (1983). The contributions of position, direction, and velocity to single unit activity in the hippocampus of freely-moving rats. *Experimental Brain Research, 52*, 41-49.

McNaughton, B.L., & Morris, R.G.M. (1987). Hippocampal synaptic enhancement and information storage within a distributed memory system. *Trends in Neurosciences, 10*, 408-415.

McNaughton, B.L., & Nadel, L. (1990). Hebb-Marr networks and the neurobiological representation of action in space. In: *Neuroscience and Connectionist Theory* (M.A. Gluck & D.E. Rumelhart, Eds.). Hillsdale, NJ: Earlbaum, pp 1-63.

Meeks, J.P., & Mennerick, S. (2007). Action potential initiation and propagation in CA3 pyramidal axons. *Journal of Neurophysiology, 97*, 3460-3472.

Miles, R., Tóth, K., Gulyás, A.I., Hájos, N., & Freund, T.F. (1996). Differences between somatic and dendritic inhibition in the hippocampus. *Neuron, 16*, 815-823.

Mistrík, P., Mader, R., Michalakis, S., Weidinger, M., Pfeifer, A., & Biel, M. (2005). The murine HCN gene encodes a hyperpolarization-activated cation channel with slow kinetics and unique response to cyclic nucleotides. *The Journal of Biological Chemistry, 280*, 27056-27061.

Mori, M., Abegg, M.H., Gähwiler, B.H., & Gerber, U. (2004). A frequency-dependent switch from inhibition to excitation in a hippocampal unitary circuit. *Nature, 431*, 453-456.

Narayanan, R., & Johnston, D. (2008). The h channel mediates location dependence and plasticity of intrinsic phase response in rat hippocampal neurons. *The Journal of Neuroscience, 28*, 5846-5860.

Noma, A., & Irisawa, H. (1976). Membrane currents in the rabbit sinoatrial node cell as studied by the double microelectrode method. *Pflügers Archives, 364*, 45-52.

Nusser, Z. (2009). Variability in the subcellular distribution of ion channels increases neuronal diversity. *Trends in Neurosciences, 32*, 267-274.

O'Reilly, R.C., & McClelland, J.L. (1994). Hippocampal conjunctive encoding, storage, and recall: Avoiding a trade-off. *Hippocampus, 4*, 661-682.

Pape, H-C. (1996). Queer current and pacemaker: The hyperpolarization-activated cation current in neurons. *Annual Review of Physiology, 58*, 299-327.

Parra, P., Gulyás, A.I., & Miles, R. (1998). How many subtypes of inhibitory cells in the hippocampus? *Neuron, 20*, 983-993.

Perez-Rosello, T., & Barrionuevo, G. (2007). Bidirectional changes in synaptic plasticity at the recurrent collateral input to stratum lacunosum molecular interneurons in hippocampal area CA3. *Society for Neuroscience Meeting*, San Diego, 362.19/M12.

Pike, F. G., Goddard, R.S., Suckling, J.M., Ganter, P., Kasthuri, N., & Paulsen, O. (2000). Distinct frequency preferences of different types of rat hippocampal neurons in response to oscillatory input currents. *Journal of Physiology, 529*, 205-213.

Pouille, F., & Scanziani, M. (2001). Enforcement of temporal fidelity in pyramidal cells by somatic feed-forward inhibition. *Science, 293*, 1159-1163.

Proenza, C., Angoli, D., Agranovich, E., Macri, V., & Accili, E.A. (2002). Pacemaker channels produce an instantaneous current. *Journal of Biological Chemistry, 277*, 5101-5109.

Proenza, C., & Yellen, G. (2006). Distinct populations of HCN pacemaker channels produce voltage-dependent and voltage-independent currents. *Journal of General Physiology, 127*, 183-190.

Puil, E., Gimbarzevsky, B., & Miura, R.M. (1986). Quantification of membrane properties of trigeminal root ganglion neurons in guinea pigs. *Journal of Neurophysiology, 55*, 995-1016.

Rall, W. (1977). Core conductor theory and cable properties of neurons. In: *Handbook of Physiology, Cellular Biology of Neurons* (E.R. Kandel, J.M. Brookhardt, & V.M. Mountcastle, Eds.). Bethesda, MD: American Physiological Society, pp 39-97.

Robinson, R.B., & Seigelbaum, S.A. (2003). Hyperpolarization-activated cation currents: From molecules to physiological function. *Annual Review of Physiology, 65*, 453-480.

Rodrigues, A.R.A., & Oertel, D. (2006). Hyperpolarization-activated currents regulate excitability in stellate cells of the mammalian ventral cochlear nucleus. *Journal of Neurophysiology, 95*, 76-87.

Rolls, E.T. (1989). Functions of neuronal networks in the hippocampus and neocortex in memory. In: *Neural Models of Plasticity* (J.H. Byrne & W.O. Berry, Eds.). San Diego: Academic Press, pp 240-265.

Rolls, E.T., & Treves, A. (1998). *Neural Networks and Brain Function*. New York: Oxford University Press.

Santoro, B., Chen, S., Lüthi, A., Pavlidis, P., Shumyatsky, G.P., Tibbs, G.R., & Seigelbaum, S.A. (2000). *The Journal of Neuroscience, 20*, 5264-5275.

Santoro, B., Liu, D.T., Yao, H., Bartsch, D., Kandel, E.R., Siegelbaum, S.A., & Tibbs, G.R. (1998). Identification of a gene encoding a hyperpolarization-activated pacemaker channel of brain. *Cell, 93*, 717-729.

Santoro, B., & Tibbs, G.R. (1999). The HCN gene family: Molecular basis of the hyperpolarization-activated pacemaker channels. *Annals of the New York Academy of Sciences, 868*, 741-764.

Seifert, R., Scholten, A., Gauss, R., Mincheva, A., Lichter, P., & Kaupp, U.B. (1999). Molecular characterization of a slowly gating human hyperpolarization-activated channel predominantly expressed in thalamus, heart, and testis. *Proceedings of the National Academy of Sciences, 96*, 9391-9396.

Shadlen, M.N., & Newsome, W.T. (1994). Noise, neural codes and cortical organization. *Current Opinion in Neurobiology, 4*, 569-579.

Softky, W.R. (1995). Simple codes versus efficient codes. *Current Opinion in Neurobiology, 5*, 239-247.

Slawínska, U., & Kasicki, K. (1998). The frequency of rat's hippocampal theta rhythm is related to the speed of locomotion. *Brain Research, 796*, 327-331.

Solomon, J.S., & Nerbonne, J.M. (1993a). Hyperpolarization-activated currents in isolated superior colliculus-projecting neurons from rat visual cortex. *Journal of Physiology, 462*, 393-420.

Solomon, J.S., & Nerbonne, J.M. (1993b). Two kinetically distinct components of hyperpolarization-activated currents in rat superior colliculus-projecting neurons. *Journal of Physiology, 469*, 291-313.

Spruston, N. (2008). Pyramidal neurons: dendritic structure and synaptic integration. *Nature Reviews Neuroscience, 9*, 206-221.

Spruston, N., Stuart, G., & Häusser, M. (1999). Dendritic integration. In: *Dendrites* (G. Stuart, N. Spruston, & M. Häusser, Eds.). Oxford University Press, pp 231-270.

Spruston, N., & Johnston, D. (1992). Perforated patch-clamp analysis of the passive membrane properties of three classes of hippocampal neurons. *Journal of Neurophysiology, 67*, 508-529.

Tamás, G., Szabadics, J., & Somogyi, P. (2002). Cell type- and subcellular position-dependent summation of unitary postsynaptic potentials in neocortical neurons. *The Journal of Neuroscience, 22*, 740-747.

Toledo-Rodriguez, M., Blumenfeld, B., Wu, C., Luo, J., Attali, B., Goodman, P., & Markram, H. (2004). Correlation maps allow neuronal electrical properties to be predicted from single-cell gene expression profiles in rat neocortex. *Cerebral Cortex, 14*, 1310-1327.

Treves, A., & Rolls, E.T. (1992). Computational constraints suggest the need for two distinct input systems to the hippocampal CA3 network. *Hippocampus, 2*, 189-200.

Treves, A., & Rolls, E.T. (1994). Computational analysis of the role of the hippocampus in memory. *Hippocampus, 4*, 374-391.

Van Wellie, I., Remme, M.W.H., van Hooft, J.A., & Wadman, W. (2006). Different levels of I_h determine distinct temporal integration in bursting and regular-spiking neurons in rat subiculum. *Journal of Physiology, 576*, 203-214.

Vida, I., & Frotscher, M. (2000). A hippocampal interneuron associated with the mossy fiber system. *Proceedings of the National Academy of Sciences, 3*, 1275-1280.

Viscomi, C., Altomare, C., Bucchi, A., Camatini, E., Baruscotti, M., Moroni, A., & DiFrancesco, D. (2001). C terminus mediated control of voltage and cyclic nucleotide-gated channels. *The Journal of Biological Chemistry, 276*, 29930-29934.

Wilent, W.B., & Contreras, D. (2006). Synaptic responses to whisker deflections in rat barrel cortex as a function of cortical layer and stimulus intensity. *The Journal of Neuroscience, 24*, 3985-3998.

Williams, S.R., & Stuart, G.J. (2000). Site independence of EPSP time course is mediated by dendritic I_h in neocortical pyramidal neurons. *Journal of Neurophysiology, 83*, 3177-3182.

Wu, JP., & Hablitz, J.J. (2005). Cooperative activation of D_1 and D_2 dopamine receptors enhances a hyperpolarization-activated inward current in layer I interneurons. *The Journal of Neuroscience, 25*, 6322-6328.

Yamada, R., Kuba, H., Ishii, T.M., & Ohmori, H. (2005). Hyperpolarization-activated cyclic nucleotide-gated cation channels regulate auditory coincidence detection in nucleus laminaris of the chick. *The Journal of Neuroscience, 25*, 8867-8877.

Yan, H., Li, Q., Fleming, R., Madison, R.D., Wilson, W.A., & Swartzwelder, H.S. (2009). Developmental sensitivity of hippocampal interneurons to ethanol: Involvement of the hyperpolarization-activated current, I_h. *Journal of Neurophysiology, 101*, 67-83.